Contributions to Mineralogy and Petrology (2020) 175:86
https://doi.org/10.1007/s00410-020-01726-9

ORIGINAL PAPER

Equilibrium crystallization of massif-type anorthosite residual melts: a case study from the 1.64 Ga Ahvenisto complex, Southeastern Finland

Riikka Fred[1] · Aku Heinonen[1] · Jussi S. Heinonen[1]

Received: 6 February 2020 / Accepted: 8 August 2020

Abstract

Fe–Ti–P-rich mafic to intermediate rocks (monzodiorites and oxide–apatite–gabbronorites, OAGNs) are found as small intrusions in most AMCG (anorthosite–magnerite–charnokite–granite) suites. The origin of the monzodioritic rocks is still debated, but in many studies, they are presumed to represent residual liquid compositions after fractionation of anorthositic cumulates. In the 1.64 Ga Ahvenisto complex, SE Finland, monzodioritic rocks occur as minor dike-like lenses closely associated with anorthositic rocks. We report new field, petrographic, and geochemical (XRF, ICP-MS, EMPA) data complemented with crystallization modeling (rhyolite-MELTS, MAGFRAC) for the monzodioritic rocks, apatite–oxide–gabbronorite, and olivine-bearing anorthositic rocks of the Ahvenisto complex. The presented evidence suggest that the monzodioritic rocks closely represent melt compositions while the apatite–oxide–gabbronorite and olivine-bearing anorthositic rocks are cumulates. The monzodioritic rocks seem to form a liquid line of descent (LLD) from primitive olivine monzodiorites to more evolved monzodiorites. Petrological modeling suggests that the interpreted LLD closely corresponds to a residual melt trend left after fractional crystallization (FC) and formation of the cumulate anorthositic rocks and minor apatite–oxide–gabbronorite in shallow magma chambers. Consequent equilibrium crystallization (EC) of separate monzodioritic residual magma batches can produce the observed mineral assemblages and the low Mg numbers measured from olivine ($Fo_{25–45}$) and pyroxenes ($En_{48–63}$, $Mg\#^{cpx}$ 60–69). The monzodioritic rocks and apatite–oxide–gabbronorites show similar petrological and geochemical characteristics to corresponding rock types in other AMCG suites, and the model described in this study could be applicable to them as well.

Keywords Massif-type anorthosites · Monzodiorites · Mineral-melt equilibrium · Crystallization modeling

Introduction

Despite decades of study of the parental magma compositions, tectonic setting, and temporal constraints of the Proterozoic massif-type anorthosites and related rock types, a consensus on their origin has not been reached (e.g., Ashwal 2010; Ashwal and Bybee 2017). Massif-type anorthosites are often associated with mangerite–charnokite–granite (AMCG; e.g., Morse 1982; Ashwal 1993) complexes with three broad lithological groups: (1) anorthosites and mafic rocks, (2) monzodioritic rocks, also referred to as ferrodiorites, jotunites, ferrogabbros, monzonorites, and (3) granitoids (e.g., Emslie 1978; Emslie et al. 1994). Based on the IUGS classification (Le Maitre et al. 2002), in this study we prefer the use of monzodiorite for the rocks in group 2.

Regarding the source of the anorthosite parental magmas, there are two main schools of thought: the advocates of (1) mantle (e.g., Emslie 1978; Mitchell et al. 1995; Frost and Frost 1997) and (2) lower crustal origins (e.g., Duchesne et al. 1999). Regardless of the penultimate source, formation of anorthosite suites is presumed to have undergone at least two stages (Ashwal and Bybee

Communicated by Mark S. Ghiorso.

Electronic supplementary material The online version of this article (https://doi.org/10.1007/s00410-020-01726-9) contains supplementary material, which is available to authorized users.

✉ Riikka Fred
riikka.fred@helsinki.fi

[1] Department of Geosciences and Geography, University of Helsinki, Gustaf Hällströminkatu 2, PL64, 00014 Helsinki, Finland

Published online: 28 August 2020

2017). First is the accumulation of buoyant plagioclase in deep magma reservoirs, which is followed by continuous, polybaric crystallization and ascent of the low-density plagioclase mushes to emplacement and final crystallization levels at 5–10 km depth in the upper crust (e.g., Ashwal 1993; Duchesne et al. 1999; Charlier et al. 2010; Bybee and Ashwal 2015). Most studies of anorthosites also agree that their parental magmas have undergone significant assimilation of crustal material, which is evident in the isotopic signatures of the resultant rock types (e.g., Mitchell et al. 1995; Heinonen et al. 2015) and that their formation involved several magma pulses (Ashwal and Twist 1994). The granitic rocks are considered either to be consanguineous with the anorthositic rocks (e.g., Frost and Frost 1997) or to comprise a separate lithological group, usually associated with lower crustal origins (Emslie et al. 1994; Ashwal and Bybee 2017).

Despite the focus of most previous studies on anorthosite petrogenesis, the monzodioritic rocks have also received warranted research interest since they are likely to bear key evidence on the petrogenesis of AMCG suites (e.g., de Waard and Romey 1969; Duchesne et al. 1974; Demaiffe and Hertogen 1981; Ashwal 1982; Duchesne 1984; Owens and Dymek 1992; McLelland et al. 1994; Mitchell et al. 1996; Markl 2001; Fred et al. 2019). The amount of monzodioritic rocks is usually minor relative to the other rock types in AMCG suites, and they are observed as dikes or other small intrusions in the contacts of associated anorthositic rocks or between the anorthositic and granitic rocks (Duchesne 1984). Whereas the anorthositic group consist of coarse-grained plagioclase cumulates that are far from melt compositions, the monzodiorites are usually fine-grained, contain more mafic minerals, and are often thus presumed to represent near melt compositions (e.g., Emslie et al. 1994; Markl and Frost 1999). In addition to high Fe, Ti, and P, the monzodiorites have low Mg-numbers and low SiO_2, and moderate to low Al_2O_3 (Duchesne 1984).

Although the monzodioritic rocks usually show uniform field, mineralogical, and geochemical characteristics, several options for their origin and relationship with the anorthosites have been proposed. They either represent (1) anorthosite parental magmas (e.g., Duchesne et al. 1974; Duchesne and Demaiffe 1978; Demaiffe and Hertogen 1981), (2) residual magmas after anorthosite fractionation (e.g., Ashwal 1982; Morse 1982; Duchesne 1984; Owens and Dymek 1992; McLelland et al. 1994; Mitchell et al. 1996; Vander Auwera et al. 1998; Dymek and Owens 2001; Markl 2001; Heinonen et al. 2010b), (3) intermediate derivatives in the evolution from anorthosite to magnerite (e.g., de Waard and Romey 1969; Philpotts 1981), (4) derivatives from mangeritic magmas (e.g., Emslie 1975; Duchesne et al. 1989), (5) immiscible liquids formed after plagioclase fractionation (e.g., Philpotts 1981), or (6) later intrusions of coeval but not comagmatic magmas with the anorthosites (e.g., Emslie 1978; Duchesne et al. 1990).

Oxide–apatite–gabbronorites (OAGN) are also found as dikes or other small intrusions in many anorthosite suites and are grouped together with the monzodiorites in some studies (see McLelland et al. 1994). These rocks are low in SiO_2 (27–42 wt%), high in TiO_2 (4–10 wt%), FeO^{tot} (17–38 wt%), and P_2O_5 (3–6 wt%), but have low K_2O (Owens and Dymek 1992). The Al_2O_3 content varies in respect to the amount of plagioclase (e.g., Owens and Dymek 1992). As their name suggest, OAGNs contain significant amounts of Fe–Ti-oxides, apatite, and also mafic phases (pyroxenes ± olivine, e.g., McLelland et al. 1994; Dymek and Owens 2001). Based on the high apatite content and enrichment in incompatible elements, they are presumed to represent a late-stage, highly differentiated magma fraction in the evolution of massif-type anorthosite suites (e.g., McLelland et al. 1994; Mitchell et al. 1996), although Dymek and Owens (2001) have suggested that OAGNs can form at several stages during the magmatic evolution of AMCG suites. Texturally, OAGNs are diverse and range from cumulates to finer-grained rocks (e.g., McLelland et al. 1994; Mitchell et al. 1996). In this study, the oxide–apatite-rich gabbronorites (OAGNs) are considered separately from the monzodioritic rocks and since the sample of this study contains more oxide it is hereafter referred as apatite–oxide–gabbronorite.

The Ahvenisto complex in southeastern Finland (Fig. 1) is one of the key locations for Fennoscandian massif-type anorthosite studies (Alviola et al. 1999; Heinonen et al. 2010a, b, 2015, 2020; Heinonen 2012; Fred et al. 2019), as it is the best representative of AMCG suite rocks at the current level of exposure in Finland (e.g., Rämö 1991). Recent studies in the Ahvenisto complex area have focused on the mantle vs. crustal sources of the complex (Heinonen et al. 2010b, 2015), the physical and chemical interactions of the associated monzodioritic and granitic magmas (Fred et al. 2019), and the polybaric crystallization history of the Ahvenisto anorthosite (Heinonen et al. 2020). Heinonen et al. (2010b) and Fred et al. (2019) preliminarily suggested that the monzodioritic rocks may approximate melt compositions and form trends that could be interpreted as a liquid line of descent (LLD) of the residual melt left after fractional crystallization of the anorthositic cumulates. In this study, we test this hypothesis by examining further petrographic and geochemical evidence together with crystallization modeling to evaluate the role of different modes of crystallization (fractional vs. equilibrium) in the formation of various rock types of the Ahvenisto complex. We compare our data and models to a global compilation of monzodioritic rocks and OAGNs and discuss the various hypotheses for the origin of the monzodioritic rocks.

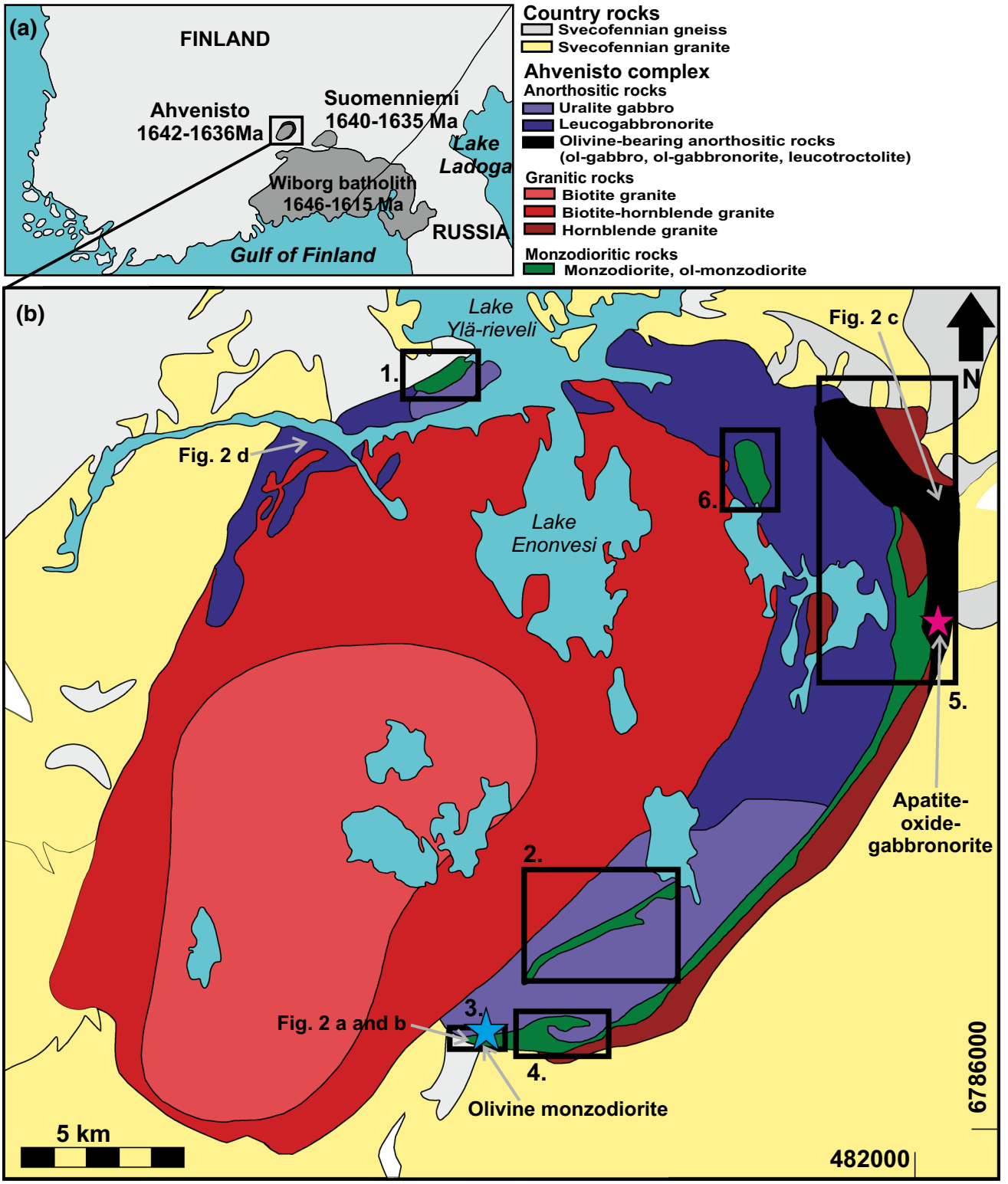

Fig. 1 **a** The location of the Ahvenisto complex in southeastern Finland, and **b** a simplified lithological map of the complex. Field work areas of this study are indicated with rectangles: (1) Tuuliniemi, (2) Pökölä, (3) Iso Kuoppalampi, (4) Pärnäjärvi, (5) Eastern part, and (6) Pitkäjärvi. The location of olivine monzodiorites and apatite–oxide-rich anorthositic rock (apatite–oxide–gabbronorite) are indicated with star symbols. The locations of the outcrop photos in Fig. 2 are also indicated [Modified after Fred et al. (2019)]

Geological background

The 1.64-Ga Ahvenisto complex

The 1.64-Ga Ahvenisto AMCG complex (Savolahti 1956, 1966; Johanson 1984; Alviola et al. 1999; Heinonen et al. 2010b, 2015, 2020) belongs to the Fennoscandian rapakivi suite (e.g., Rämö and Haapala 2005; Rämö et al. 2014) and is located northwest of the Wiborg batholith in southeastern Finland (Fig. 1). At the current level of exposure, the granitic rocks dominate the rapakivi suite, and only a small amount of anorthositic and mafic rocks are present as dikes or other small intrusions (e.g., Eklund 1993; Alviola et al. 1999; Rämö and Haapala 2005; Heinonen et al. 2010a, b; Fred et al. 2019). The Ahvenisto complex intruded the Svecofennian (1.9–1.8 Ga) country rocks and the crystallization ages of the different rock types vary from 1643 to 1632 Ma (Heinonen et al. 2010b). The complex comprises a granitic intrusion (ca. 70% of areal extent) surrounded by an anorthositic arc (25%) that includes volumetrically minor monzodioritic rocks found as dike-like lenses (5% of the area, e.g. Savolahti 1956, 1966; Johanson 1984; Alviola et al. 1999; Heinonen et al. 2010b; Fred et al. 2019)—the usual lithological assemblage of AMCG complexes (Emslie et al. 1994). Field relations suggest that the anorthositic rocks are the oldest of the mafic rocks and monzodioritic rocks are the youngest (Alviola et al. 1999). The granitic rocks are dominantly younger than all the mafic rocks (Alviola et al. 1999), but mingling structures have been reported as evidence of simultaneous emplacement of the monzodioritic and the earliest granitic melts (Fig. 2a; Fred et al. 2019).

Hafnium, Nd, Sr, and O isotope data indicate a depleted upper mantle origin for the parental magmas of the anorthositic rocks (e.g., Heinonen et al. 2010a, b). The anorthositic rocks themselves display a largely crustal isotope signature, likely resulting from assimilation of crustal

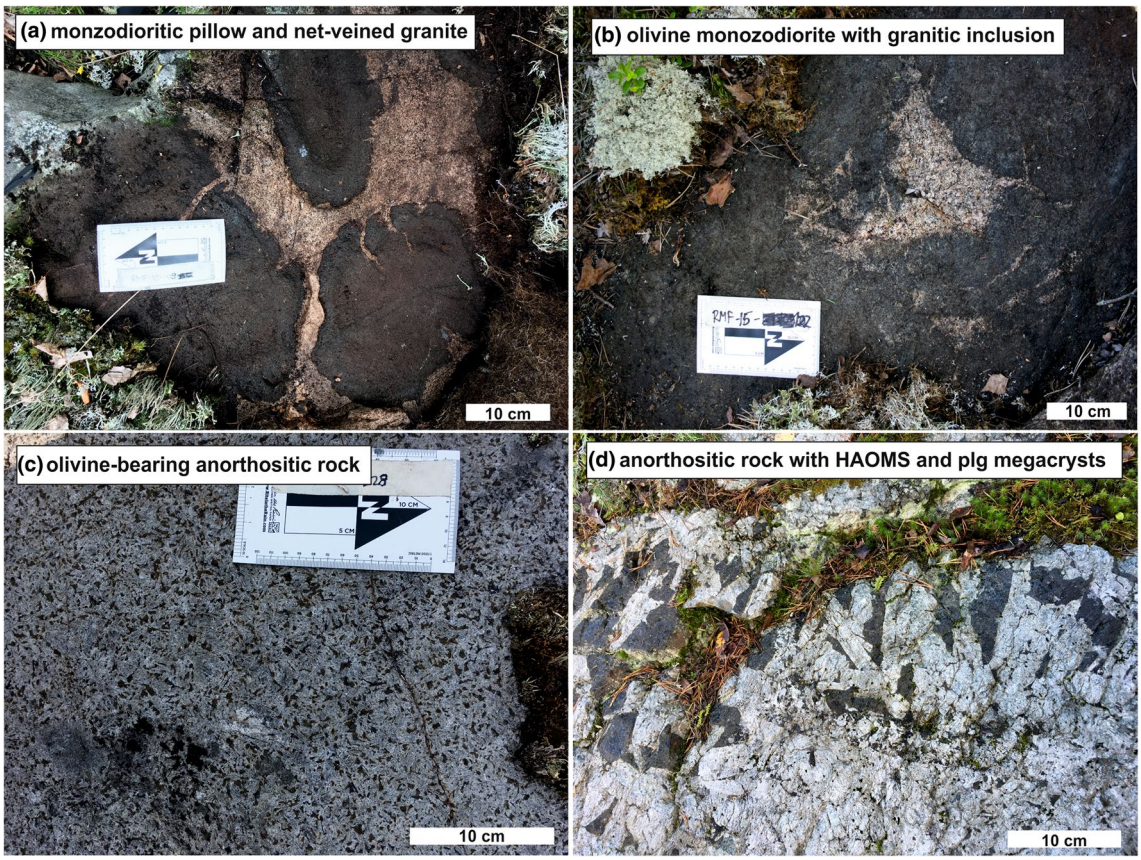

Fig. 2 Outcrop photos showing some typical features of the different rock types in the Ahvenisto complex: **a** fine-grained (< 1 mm) monzodioritic material mingled with granitic material in pillow and net-veined structures, **b** fine- to medium-grained (< 1–5 mm) olivine monzodiorite with granitic inclusion, **c** coarse-grained olivine-bearing anorthositic rock with cumulus plagioclase (~ 1 cm) and interstitial mafic material, and **d** coarse-grained anorthositic rock with a pocket of orthopyroxene (HAOM) and plagioclase megacrysts (up to 10 cm). **a** and **b** are from the Iso Kuoppalampi area, **c** from the north eastern area, and **d** is located southwest from the Tuuliniemi area (Fig. 1)

materials (e.g., Heinonen et al. 2010a, b, 2015). The granitic magmas of the suite were produced from partial melts of the lower crust with a possible minor mantle component (e.g., Heinonen et al. 2010a, 2015). Nd–Sr isotopes suggest a comagmatic origin for the anorthositic (initial ε_{Nd} − 0.9 to − 0.5 and Sr 0.7037 to 0.7041) and monzodioritic rocks (initial ε_{Nd} − 1.1 to − 0.2 and Sr 0.7028 to 0.7040; Heinonen et al. 2010b). Al-in-opx geobarometry suggests that the anorthositic rocks crystallized polybarically at three different levels: (1) high-P conditions in lower crust (~ 1100 MPa), (2) mid crustal levels (~ 500 MPa), and (3) upper crustal levels (~ 200 MPa) (Heinonen et al. 2020).

Rock types of the Ahvenisto complex

Anorthositic rocks

The anorthositic arc of the complex that consists mainly of leucogabbronorites with minor uralite gabbro (gabbro in which clinopyroxene is replaced by amphibole; Fig. 3f) in the southern parts and a small lens of olivine–gabbronorites, olivine–gabbros, and leucotroctolites in the northeastern corner of the arc (Savolahti 1956, 1966; Johanson 1984; Alviola et al. 1999; Heinonen et al. 2010b). Anorthosite, sensu stricto, only occurs as small lenses (200 m at widest) and inclusions. Minor amounts of pegmatitic and ilmenite gabbro are scattered throughout the anorthositic arc (Alviola et al. 1999). All these rock types represent leucocratic plagioclase cumulates and are hereafter referred to as anorthositic rocks (anorthosite, leucogabbronorite, uralite gabbro, ilmenite gabbro) and olivine-bearing anorthositic rocks (olivine–gabbronorite, olivine–gabbro, leucotroctolite).

The leugogabbronorite consists of coarse-grained (0.5–2 cm) plagioclase and interstitial mafic minerals (10–25 vol%; Alviola et al. 1999). The olivine-bearing anorthositic rocks in the northeastern part are usually subophitic to ophitic with coarse plagioclase (0.5–2 cm; Fig. 2c). They are texturally similar to the leugogabbronorites, but the amount of mafic minerals is higher (20–45 vol%). The anorthosite lenses consist of medium- to coarse-grained equigranular to sparsely megacrystic plagioclase, which is locally foliated (Alviola et al. 1999), and the amount of mafic minerals is minor (< 10 vol%). The contact of the anorthosite lenses to leucograbbronorites is usually sharp (Alviola et al. 1999). Plagioclase in all anorthositic rocks is euhedral and associated with usually interstitial mafic minerals (clino- and orthopyroxene ± olivine; Fig. 3e, f), but olivine is occasionally sub- to euhedral (Alviola et al. 1999). Ilmenite is a common accessory phase (Alviola et al. 1999). Large (up to 30 cm long) orthopyroxene (high aluminum orthopyroxene megacrysts = HAOM) and associated plagioclase megacrysts usually ~ 10 cm (up to 50 cm) long are found in several locations throughout the anorthositic arc (Fig. 2d, e.g., Savolahti 1966; Alviola et al. 1999; Heinonen et al. 2020).

Monzodioritic rocks

The monzodioritic rocks are usually exposed between the outer rim of the anorthositic arc and either the hornblende granites (southeastern part) or the Svecofennian country rocks (northwestern part; Fig. 1). A small lens of monzodioritic rocks is found inside the anorthositic arc in the northeastern corner of the complex (Fig. 1; Pitkäjärvi area). The monzodioritic dike-like lenses mostly consist of (1) fine- to medium-grained (< 1–3 mm) massive monzodiorite with poikilitic hornblende phenocrysts or (2) fine-grained (< 0.5 mm) monzodiorite as pillow-like structures mingled with net-veined granitic material (Fig. 2a; Johanson 1984; Alviola et al. 1999; Fred et al. 2019). The granitic material involved in the mingling structures is presumed to be associated with the marginal hornblende granites (Fig. 1) and evidence of mixing of these two magma types has also been observed in hybrid rocks (Fred et al. 2019). Also, a small lens (~ 200 m wide) of (3) medium-grained (1–5 mm) and dark olivine–monzodiorite is found in the southern part of the complex (Figs. 1, 2b; Iso Kuoppalampi area; Fred et al. 2019).

The massive monzodiorite (Fig. 3b) consists of fine-grained groundmass of plagioclase, pyroxenes, and K-feldspar with minor amounts of quartz and biotite (Fred et al. 2019). Poikilitic hornblende crystals stand out from the groundmass (Fig. 3b). Typical accessory phases are oxide, apatite, and zircon. The pillow-type monzodiorite (Fig. 3a) consists of fine-grained groundmass of plagioclase, amphibole, biotite, and K-feldspar, and minor amounts of oxide and apatite (Fred et al. 2019). Quartz is an accessory phase. Plagioclase phenocrysts and amphibole pseudomorphs (replacing pyroxene) stand out from the groundmass (Fig. 3a). A few fresh pyroxene phenocrysts are present (Fred et al. 2019).

Geochemically, the Ahvenisto monzodioritic rocks seem to form an evolutionary trend from olivine monzodiorite through pillow type-monzodiorite to massive monzodiorite (Fred et al. 2019). The contact between the monzodioritic rocks and the anorthositic cumulate rocks, where visible, is either (1) sharp and monzodiorite shows chilled margins (Alviola et al. 1999), (2) locally gradational in wide scale, or (3) complex with sheets of granitic, and country rock material brecciated by monzodioritic and anorthositic rocks (Fred et al. 2019). The monzodioritic rocks are hereafter referred to as monzodiorites (pillow-type monzodiorites and massive monzodiorites) and olivine monzodiorites.

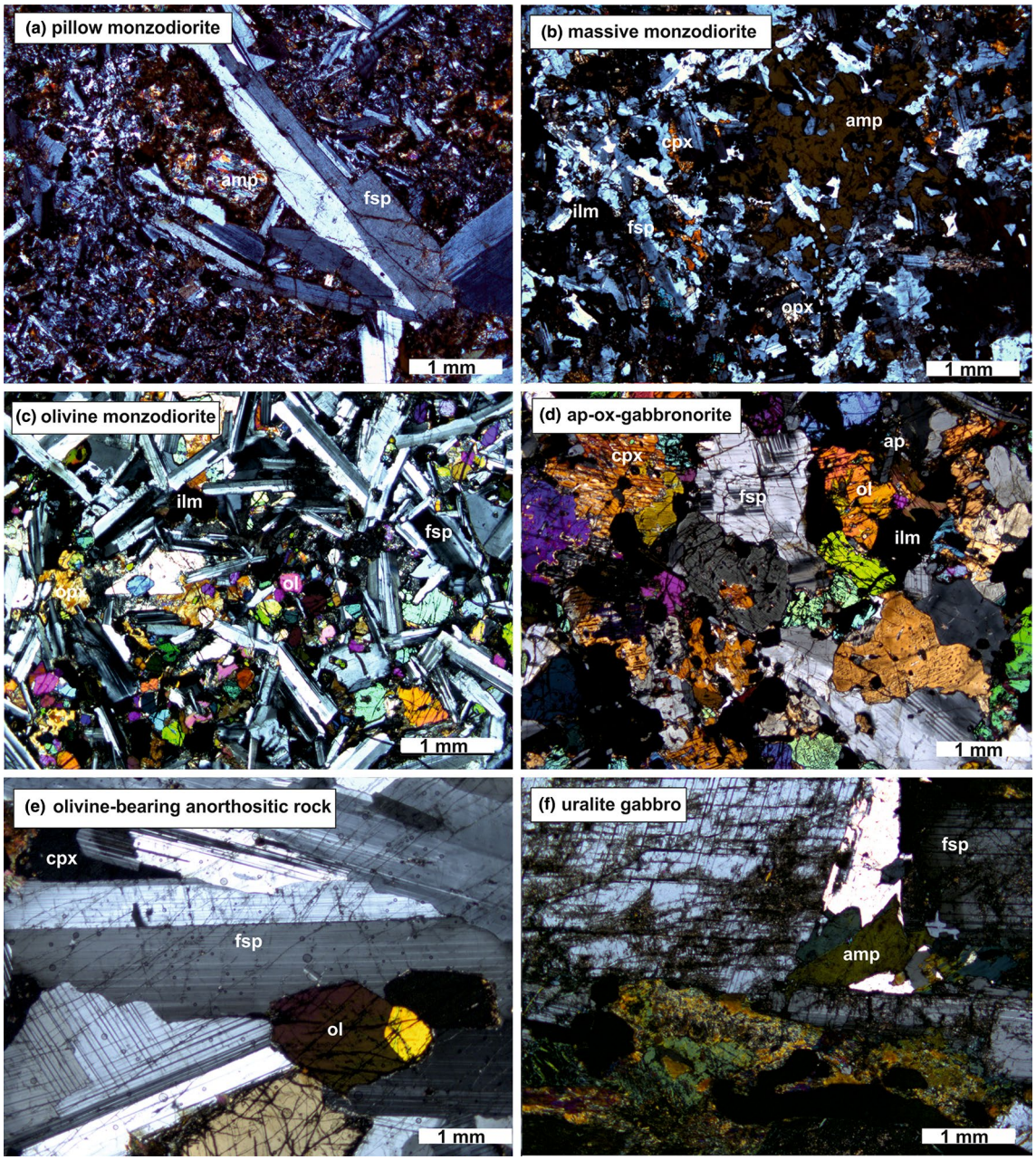

Fig. 3 Thin-section photomicrographs of **a** pillow monzodiorite (see Fred et al. 2019), **b** massive monzodiorite (see Fred et al. 2019), **c** olivine monzodioritie (RMF-18-249), **d** apatite–oxide–gabbronorite (RMF-18-129), **e** olivine-bearing anorthositic rock (RMF-18-211), and **f** uralite gabbro (see Fred et al. 2019) in cross-polarized light. The monzodioritic rocks have fine-grained groundmass (pillows < 0.1 mm, massive < 0.5 mm, olivine monzodiorite < 1 mm). The monzodiorite pillows and olivine monzodiorite contain plagioclase phenocrysts (1–10 mm) and the former also amphibole pseudomorphs. Poikilitic amphibole is common in massive monzodiorite. In contrast, the anorthositic rocks (**e**, **f**) are coarse-grained (< 1 cm) and consist of cumulus plagioclase with usually interstitial mafic minerals (20–40 vol%). The apatite–oxide–gabbronorite is medium-grained (1–10 mm) and contains high amount of mafic minerals (~ 50 vol%), ilmenite, and apatite. Abbreviations are according to Whitney and Evans (2010)

Methods and materials

Much of the field observations that form the basis of this study were performed and reported in Fred et al. (2019), but also some complementary field work was conducted and is discussed in the results section below. During the field work, monzodioritic rocks (eight monzodiorite and eight olivine monzodiorite samples), olivine-bearing anorthositic rocks (three samples), and apatite–oxide–gabbronorite (one sample) were sampled with a hammer for petrography,

whole-rock major and trace element geochemistry (X-ray fluorescence, XRF, and inductively coupled plasma mass spectrometry, ICP-MS), and major element mineral chemistry (electron microprobe analyzer, EMPA). The 20 new samples and 15 samples from Fred et al. (2019) were analyzed for whole-rock geochemistry. A more detailed petrographic study of 12 new samples was conducted and nine olivine-bearing samples (six olivine monzodiorites, two olivine-bearing anorthositic rocks, and one apatite–oxide–gabbronorite) were selected for mineral chemical analysis. All sample preparation stages were conducted at the Mineralogical Laboratory of the University of Helsinki.

XRF and ICP-MS analyses

Whole-rock samples were prepared with a rock saw to avoid any weathering surfaces and crushed with a jaw crusher (minor contamination with Fe, Cr, Ni, and V is possible). Representative pieces were handpicked to avoid altered and weathered parts. The whole-rock XRF and ICP-MS analyses for the 20 new samples were conducted at the Geoscience Laboratories, Ontario, Canada. The samples were pulverized in a 99.8% Al_2O_3 planetary ball mill (minor contamination with Al) and run for LOI in 105 °C under nitrogen atmosphere and 1000 °C under oxygen atmosphere. The calcined samples were fused with a borate flux to produce glass beads for the XRF analyses (Hargreaves 2015). The deviation from standard is < 3% for all major elements. The coefficient of variation is < 2%. The preparation of samples for ICP-MS was conducted using closed vessel multi-acid digestion method for complete dissolution (Hargreaves 2017). The deviation from standard is ≤ 5% for most of the trace elements, except Nb (6%), Hf (8%), Cs (15%), Pb (17%), Tb (24%), Er (9%), Tm (23%), Lu (12%), and Li (6%). The coefficient of variation is ≤ 5% for most of the trace elements, except Ni (8%) and Pb (6%).The 15 previously analyzed samples (Fred et al. 2019) were reanalyzed for major and trace element compositions at the USGS laboratories. Sample preparation procedures for these samples are described in Fred et al. (2019) and analytical details follow those described in Taggart and Siems (2002). The deviation from standard is ≤ 2% for all major elements analyzed with XRF, except for MnO (6%). The coefficient of variation for major elements is ≤ 2%. The deviation from standard is ≤ 5% for most of the trace elements analyzed with ICP-MS, except for Cr (13%), Ni (8%), Cu (11%), Ta (11%), Nb (16%), Y (9%), Tm (7%), and Yb (7%). The coefficient of variation for REE is ≤ 2% and other trace elements ≤ 15%. The whole-rock samples were also measured for ferrous iron. The 20 new samples were dissolved in an aggressive, non-oxidizing acid mixture, and the solubilized ferrous iron was quantified by potentiometric titration with a standardized permanganate solution (Hargreaves 2019). The deviation from standard is 1% for FeO and the coefficient of variation is 0.5%. The whole dataset together with standard measurements is given in Online Resource 1.

EMPA analyses

Electron microprobe analyses were conducted at the Mineralogical Laboratory of the University of Helsinki using a JEOL JXA-8600 electron microprobe analyzer (EMPA) equipped with four wavelength-dispersive (WDS) spectrometers, upgraded with SAMx analytical software and PointElectronic SAMx hardware. Six carbon-coated thin sections of olivine monzodiorite, two olivine-bearing anorthositic rocks, and one apatite–oxide–gabbronorite were selected for quantitative (WDS) major element analysis of the mineral phases. Additional qualitative (energy dispersive spectrometer, EDS) analyses were performed to identify accessory phases. An acceleration voltage of 15 kV, sample current of 15 nA, and beam size of ca. 10 µm were used for the WDS analyses. Calibration was performed using a set of natural and synthetic oxide and silicate standards. Matrix corrections for the analysis were done by the SAMx analysis software using the PAP correction. The potential Si Kβ overlap over Sr Kα has been calculated after the Si Kβ intensity at the Sr Kα peak position was measured. General precision is estimated to be about 2% for major elements (> 10 wt%) and below 5% for minor elements (1–10 wt%; Michallik et al. 2017). The whole dataset is given in Online Resource 1.

MELTS software

MELTS is a software package that facilitates thermodynamic modeling of phase equilibria in magmatic systems (Ghiorso and Sack 1995; Gualda et al. 2012). It can be used to simulate igneous processes, such as equilibrium and fractional crystallization. The most recent rhyolite-MELTS versions (Gualda et al. 2012) have been appended with H_2O–CO_2 fluid saturation models (Ghiorso and Gualda 2015) and can be used for natural silica-dominated compositions over temperatures of 500–2000 °C and pressures of 0–2 GPa. The software predicts phase equilibria (solid phases, melt, and fluid, and their major element compositions) from bulk composition of the system at, for example, given pressure–temperature conditions. The conditions can vary according to user-defined steps: decreasing temperature steps can be utilized in modeling of equilibrium (all phases stay in equilibrium) or fractional (formed solids are removed every step) crystallization.

MAGFRAC program

The MAGFRAC program of Morris (1984) is based on the least squares approximation of best-fit compositions. The

least squares approximation is based on the following: "computer estimated proportions of fractionating minerals are 'mixed' with the daughter liquid to produce the best-fit estimated parent composition. The suitability of this estimated parent composition is given by squaring the sum of differences (i.e. residuals) between the estimate and observed parent compositions" (Bryan et al. 1969). In MAGFRAC, the input includes user-defined oxide compositions of the observed parent melt, daughter melt, and presumed fractionating minerals (1–X phases; Morris 1984). The program gives estimated parent melt composition, sum of squared residuals, and mineral and daughter liquid proportions (Morris 1984).

Results

Field work

The focus of the recent field work was to gather additional and new knowledge on the most primitive olivine-bearing anorthositic rocks and monzodioritic rocks of the Ahvenisto complex. Six representative mapping locations were selected from these lithological units (Fig. 1).

As already discussed, the Ahvenisto complex hosts three different monzodiorite types: massive monzodiorite, which is the most common, pillow-type monzodiorite, and rare olivine monzodiorite (See Fred et al. 2019). Due to scarce outcrops in the assumed contact zones, the contacts between the olivine-bearing or other anorthositic rocks and monzodioritic rocks that have been described as sharp in earlier studies (Johanson 1984; Alviola et al. 1999), were not observed. Instead we found that, locally, and near the assumed contacts, the grainsize of anorthositic rocks decreased and that of monzodioritic rocks increased. This phenomenon may be related to uneven cooling of the individual intrusions in a complex setting of cold basement and still warm AMCG-related wallrocks.

The interaction structures (Johanson 1984; Alviola et al. 1999; Fred et al. 2019) were found to be much more widespread than previously reported. The mingling structures occur throughout the monzodioritic rocks and also hybrid rocks are observed in several locations in the southeastern part of the complex. The olivine monzodiorites seem to be limited to a small area near lake Iso Kuoppalampi (Fig. 1). Due to scarce outcrops, the mode of occurrence (i.e. dike or lens, etc.) of this olivine monzodiorite could not be determined, but it is presumed to represent a more mafic and coarser-grained part of the monzodioritic dike. The observed areal existence of the olivine monzodiorite is ~ 0.02 km^2.

The Ahvenisto olivine-bearing anorthositic body was found to correspond to previous descriptions: plagioclase (grainsize ~ 1 cm) cumulate rock with interstitial mafic minerals (20–40% vol%). However, this body was found to also contain lenses of pegmatitic material with compositions varying from very coarse-grained anorthositic rock with orthopyroxene megacrysts to megacrystic plagioclase–pyroxene rock. In the southern and eastern margins of the olivine-bearing anorthositic body, a medium- to coarse-grained (0.5–1 cm) cumulate rock with high amount (up to 50 vol% or more) of mafic minerals and red alteration color (usually the anorthositic rocks show light gray alteration color) was observed.

Petrography

A generalized overview of the petrography of the different rock types was provided in the "Geological background" section. Here we give more detailed descriptions that are appended with the new data and observations.

The massive monzodiorite consists of fine-grained groundmass of plagioclase, K-feldspar, quartz, and pyroxenes with poikilitic hornblende (Fig. 3a; Fred et al. 2019). The pillow-type monzodiorite consists of very fine-grained groundmass of plagioclase, K-feldspar, amphibole, and biotite with plagioclase phenocrysts and amphibole pseudomorphs (Fig. 3b; Fred et al. 2019). The olivine monzodiorite consists of euhedral and fresh plagioclase laths (0.1–1 mm) with ortho- and clinopyroxene (< 0.5 mm) and olivine (< 0.5 mm) as the other major phases (Fig. 3c). Olivine is usually subhedral and fresh. Pyroxenes are anhedral and show strong exsolution of clinopyroxene in orthopyroxene and vice versa. Plagioclase phenocrysts (up to 5 mm) are common and occasionally show normal zoning. Fe–Ti oxides (ilmenite + minor magnetite), apatite, and interstitial K-feldspar, and minor biotite and zircon are found as accessory phases. The modal amount of plagioclase in olivine monzodiorite is approximately similar to the amount of mafic phases (olivine + pyroxenes).

The olivine-bearing anorthositic rocks are dominated by cumulus plagioclase with interstitial ortho- and clinopyroxene and olivine is also found as a major phase (15–40 vol%; Fig. 3e). Fe-Ti oxides (ilmenite + minor magnetite) and biotite are common accessory phases. The grain size of plagioclase is usually ~ 1 cm but clusters of smaller (2–5 mm) grains are also observed. Some of the larger crystals show zoning. Olivine is fresh and sub- to anhedral and complex rims (consisting of, e.g., bitotite + orthopyroxene + symplectite) are common. Pyroxenes are altered and clinopyroxene exsolution lamellae in orthopyroxene and vice versa are common.

The apatite–oxide–gabbronorite consists of plagioclase, olivine, and ortho- and clinopyroxene (plg ~ 45 vol% and mafic minerals ~ 50 vol%) together with apatite (~ 5 vol%) and Fe–Ti oxides (~ 10 vol%, mostly ilmenite) as major phases (Fig. 3d). Euhedral plagioclase (0.5–1 cm) and

subhedral olivine (1–5 mm) are fresh. Anhedral pyroxenes are altered and exsolution is common. Euhedral apatite grains are up to 3 mm in size.

Whole-rock geochemistry

Representative major and trace element compositions of the whole-rock samples are illustrated in Figs. 4 and 5. The whole dataset is presented in Online Resource 1.

Major elements

The monzodioritic rocks have SiO_2 contents between 46 and 52 wt%: the olivine monzodiorites have usually < 50 wt% and the monzodiorites > 50 wt% with two exceptions that have SiO_2 of ~ 46 wt% (Online Resource 1). The MgO content of the monzodioritic rocks decreases with decreasing Mg# ($Mg^{2+}/Mg^{2+} + Fe^{2+}$), while the FeO^{tot} content remains nearly constant (Fig. 4c, d). The olivine monzodiorites show strong increase in TiO_2 and slight increase in K_2O and P_2O_5 contents and decreased MgO with decreasing Mg# (Fig. 4a, d, g, h). The monzodiorites show decrease in MgO and increase in K_2O and P_2O_5 with decreasing Mg# (Fig. 4d, g, h). The two monzodiorite samples with low SiO_2 have anomalously high TiO_2, FeO^{tot}, CaO, and P_2O_5 contents (Fig. 4a, c, e, g).

The olivine-bearing anorthositic rocks show similar SiO_2 (47–49 wt%; Online Resource 1) contents than most of the olivine monzodiorites, but higher Al_2O_3, CaO, and Na_2O and relatively lower MgO, FeO^{tot}, TiO_2, MnO, K_2O, and P_2O_5 (Fig. 4).

The apatite–oxide–gabbronorite shows the lowest SiO_2 (~ 40 wt%) and is also otherwise compositionally deviant. The sample has high TiO_2 (> 4 wt%), FeO^{tot} (> 26 wt%), MnO, and P_2O_5 (> 2 wt%) and relatively high MgO and low Al_2O_3, Na_2O, and K_2O (Fig. 4b, d, f, g). The apatite–oxide–gabbronorite and the low-SiO_2 high-TiO_2 monzodiorites form a divergent differentiation trend compared to the governing monzodioritic trend (Fig. 4).

Trace elements

The amount of most of the incompatible trace elements increase linearly with decreasing Mg# from olivine monzodiorites to the most evolved monzodiorites. All the samples show slight enrichment in LREE relative to HREE (Fig. 5a). The apatite–oxide–gabbronorite has the highest REE contents with slightly flatter LREE and steeper HREE curves than the monzodioritic rocks (Fig. 5a). The olivine-bearing anorthositic rocks show strong positive Eu anomalies (Eu/Eu* 1.58–1.88) and monzodiorites and apatite–oxide–gabbronorite negative Eu anomalies (Eu/Eu* 0.56–0.90 and 0.69, respectively). The olivine monzodiorites do not show notable Eu anomalies (Eu/Eu* 0.84–1.08). The olivine-bearing anorthositic rocks and monzodiorites show similar incompatible trace element patterns, except that the olivine-bearing anorthositic rocks are enriched in Sr while the monzodiorites and apatite–oxide–gabbronorite are depleted in Sr (Fig. 5b). The apatite–oxide–gabbronorite shows a more variable pattern. The olivine-bearing anorthositic rocks and monzodiorites are relatively enriched in Ba, K, and Zr and depleted in Ti. The monzodiorite sample with anomalously K_2O at a given Mg# (Fig. 4) is the one with the high Rb content (Fig. 5b).

Mineral chemistry

The full dataset of Ahvenisto mineral chemical compositions (for six olivine monzodiorites, two olivine-bearing anorthositic rocks, and one apatite–oxide–gabbronorite) is available in Online Resource 1. Main observations are discussed below and illustrated in Figs. 6, 7 and 8.

Plagioclase

Plagioclase composition was measured from groundmass, phenocrysts, and inclusions in pyroxenes. The groundmass plagioclase composition in the olivine-bearing anorthositic rocks varies between $An_{50–66}$, in olivine monzodiorites between $An_{48–58}$, and in the apatite–oxide–gabbronorite between $An_{40–43}$ (Fig. 6; Online Resource 1). The plagioclase inclusions in olivine monzodiorites have similar compositions ($An_{50–53}$) as groundmass plagioclase. Some of the largest phenocrysts in olivine-bearing anorthositic rocks and olivine monzodiorites show normal zoning from $An_{53–62}$ (center) to $An_{39–51}$ (rim). All analyzed plagioclase grains contain small amounts of Fe and have low Or content (≤ 4 mol%).

Olivine

The olivine composition is homogenous within samples and notable differences in composition between finer and coarser grains were not observed. However, the Fo content of olivine decreases with decreasing Mg# of the corresponding host whole rock sample (Fig. 7). The Fo content of olivine varies between $Fo_{45–53}$ in olivine-bearing anorthositic rocks, between $Fo_{25–45}$ in olivine monzodiorites, and between $Fo_{19–20}$ in apatite–oxide–gabbronorite (Fig. 7; Online Resource 1). Olivine is not in Fe–Mg equilibrium with the measured host whole-rock compositions (Fig. 9a).

Pyroxene

Orthopyroxene and clinopyroxene are usually found together in the Ahvenisto samples. The pyroxenes exhibit clear

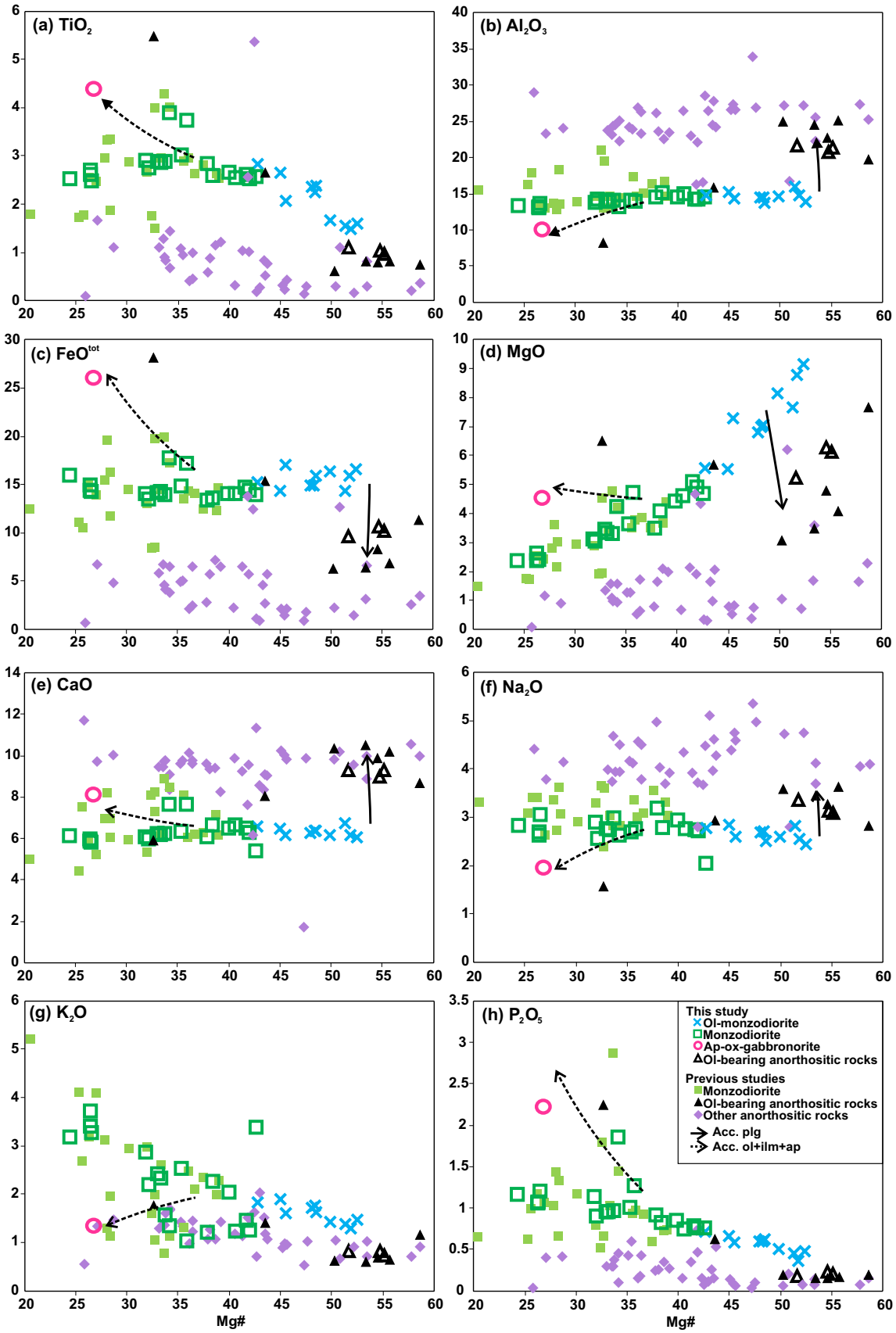
(a) TiO2
(b) Al2O3
(c) FeOtot
(d) MgO
(e) CaO
(f) Na2O
(g) K2O
(h) P2O5
Mg#
This study
Ol-monzodiorite
Monzodiorite
Ap-ox-gabbronorite
Ol-bearing anorthositic rocks
Previous studies
Monzodiorite
Ol-bearing anorthositic rocks
Other anorthositic rocks
Acc. plg
Acc. ol+ilm+ap

◂**Fig. 4** Major element variation diagrams of Mg# [Mg^{2+}/(Mg^{2+}+Fe^{2+})*100] vs. **a** TiO_2, **b** Al_2O_3, **c** FeO^{tot}, **d** MgO, **e** CaO, **f** Na_2O, **g** K_2O, and **h** P_2O_5 for the Ahvenisto complex monzodioritic rocks, olivine-bearing anorthositic rocks, and apatite–oxide–gabbronorite. The black solid arrow indicates plagioclase accumulation and black dashed arrow indicates accumulation of oxide, apatite, and olivine in 1:1:5, respectively

exsolution textures either as irregular blebs or as regular lamellae: in orthopyroxene the lamellae are clinopyroxene and vice versa. The lamellae are thin (< 10 µm) and their effects for the analyses are reflected in Fig. 8 as compositions intermediate between ortho- and clinopyroxenes. Ilmenite exsolution is also common. The En content of the orthopyroxenes in olivine monzodiorites varies between $En_{48–63}$, in olivine-bearing anorthositic rocks between $En_{56–66}$, and in apatite–oxide–gabbronorite between $En_{33–35}$ (Fig. 8; Online Resource 1). The Mg# of clinopyroxenes varies between 60 and 69 in olivine monzodiorites, 68 and 74 in olivine-bearing anorthositic rocks, and 45 and 51 in apatite–oxide–gabbronorite (Online Resource 1). The pyroxenes contain small amounts of MnO and Al_2O_3, and the clinopyroxene also contains minor amounts of Na_2O and TiO_2. As is the case with olivine, pyroxenes are not in Fe–Mg equilibrium with the measured host whole-rock composition in any of the studied rock types (Fig. 9b, c).

Discussion

This study mainly deals with the of the monzodioritic rocks in the Ahvenisto complex and their comparison to similar rocks in other anorthosite suites. Therefore, major part of the following inferences concentrate on their features and the discussion on the complementary cumulates remains more concise. The observation of apparent mineral-melt Fe–Mg disequilibrium in the olivine monzodiorites is discussed first to set the stage, followed by an outline of the overall evolution of the compositional monzodiorite evolution and their relationship with the cumulate rocks. Regardless of its relatively evolved composition, the apatite–oxide–gabbronorite of the Ahvenisto complex is not considered to belong to the monzodioritic rocks and is dealt with separately. The penultimate part of the discussion is devoted to the regional implications of the findings in context of Fennoscandian rapakivi magmatism, and finally a global comparison of the petrogenetic significance of monzodioritic rocks in AMCG complexes is briefly outlined.

Magmatic evolution of the mafic rock types of the Ahvenisto complex

Equilibrium crystallization of the monzodioritic rocks

Multiple lines of field, textural, and geochemical evidence support the hypothesis that most of the Ahvenisto monzodioritic rocks record evidence of melt compositions and that they most likely represent residual melts left after fractionation of plagioclase (± mafic minerals) during anorthositic cumulate formation—these are reviewed in detail below. The directly observed contacts between the monzodioritic and anorthositic rock are sharp and the former always cross cut the latter (Alviola et al. 1999), which establishes the later crystallization of the monzodioritic rocks relative to the cumulates. Majority of the monzodioritic rocks are fine-grained and show no textural or petrographic cumulate features. Furthermore, the major element compositions of most monzodioritic rocks show no evidence of phase accumulation (Fig. 4), except for some of the more evolved monzodiorites that deviate from the main Ahvenisto trend towards higher Al_2O_3 and CaO and lower K_2O, most likely reflecting minor accumulation of plagioclase in these samples (Figs. 4, 11). Some samples show enrichment in TiO_2 and P_2O_5 due to ilmenite and apatite accumulation, respectively. Unlike the anorthositic rocks, the monzodioritic rocks either have no Eu-anomaly (some olivine monzodiorites) or have negative Eu-anomalies suggesting that they are not plagioclase cumulates and that the more evolved monzodiorites have gone through plagioclase fractionation. The REE abundances of the monzodioritic rocks are much higher than in the anorthositic cumulates and increase from olivine monzodiorites to the monzodiorites (Fig. 5), which suggest that they represent evolving residual liquid compositions. Being interpreted as approximate melt compositions, the primitive olivine monzodiorites represent a rock type that has previously not been reported in any other AMCG complex and as such open up a new perspective in the study of parental magma compositions of massif-type anorthosites.

If the olivine monzodiorites closely represent melt compositions as we suggest, it is odd (at first sight) that neither the olivine nor pyroxenes found in them are in Fe–Mg equilibrium with the host rock (i.e., presumed melt) compositions (Fig. 9). Especially olivine shows remarkably low Mg ($Fo_{25–45}$) contents compared to what would be expected to be in equilibrium with melts that correspond to the monzodioritic rocks (Mg# 42–52, in equilibrium with $Fo_{\sim 70–80}$; Fig. 9).

To explain these abnormal, excessively evolved mineral compositions, several options were considered. Accumulation, mixing, or other xenocrystic origins seem implausible already based on the above-mentioned whole-rock geochemical evidence. There is no petrographic evidence of xenocrystic origin either: the olivine is compositionally homogenous at the scale of individual grains, does not contain reaction rims, and its crystal habit and textural features support in-situ crystallization Mass balance calculations (using MAGFRAC) using measured mineral chemistries give almost identical whole-rock compositions compared to the analyzed compositions, and the phase proportions yielded by the calculations are reasonable as well. The Fe^{3+}/

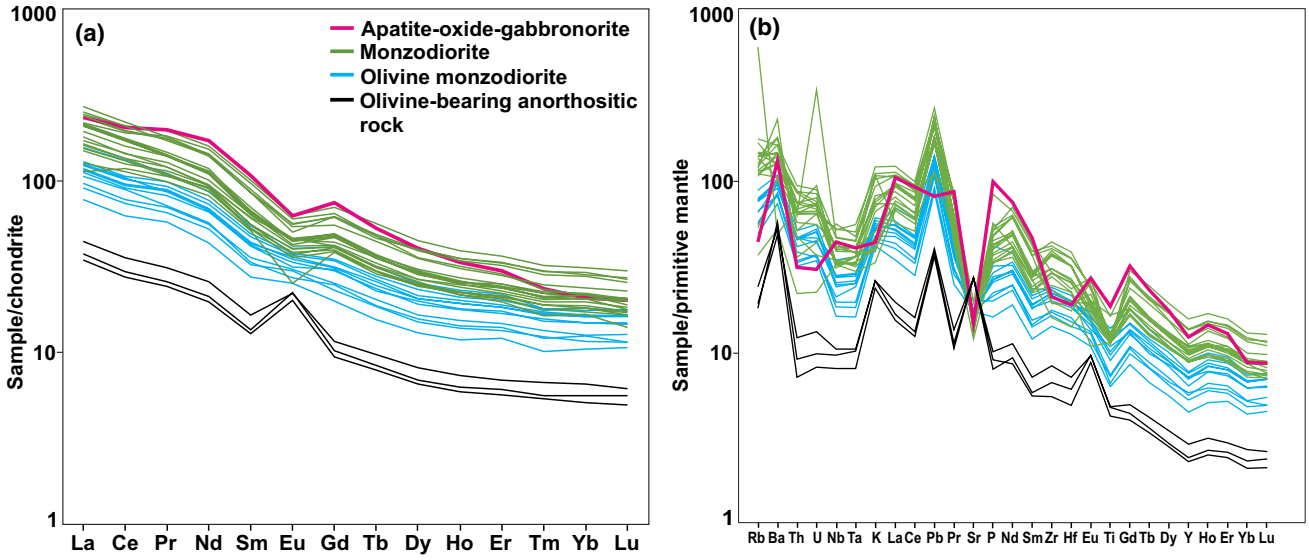

Fig. 5 **a** REE diagram normalized to chondrite (Boynton 1984) and **b** incompatible trace element diagram normalized to primitive mantle (Sun and McDonough 1989) for the Ahvenisto complex monzodioritic rocks, olivine-bearing anorthositic rocks, and apatite–oxide gabbronorite

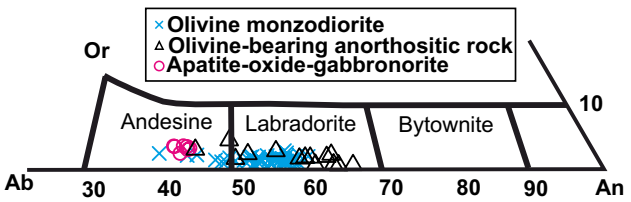

Fig. 6 An–Ab–Or classification diagram showing the plagioclase compositions of the Ahvenisto complex olivine monzodiorites, olivine-bearing anorthositic rocks, and apatite–oxide–gabbronorite

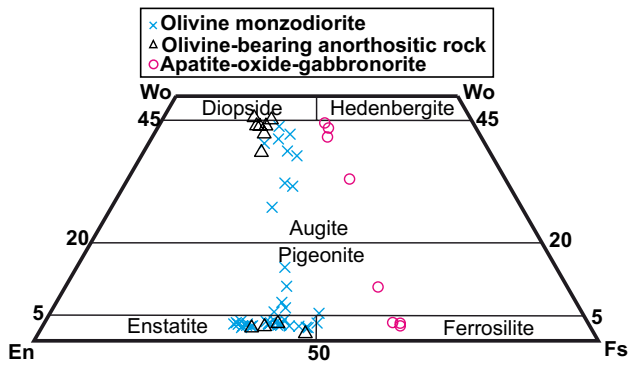

Fig. 8 Pyroxene compositions of the Ahvenisto complex olivine monzodiorites, olivine-bearing anorthositic rocks, and apatite–oxide–gabbronorite show the co-existence of two pyroxenes in all of the analyzed samples. The effect of strong exsolution of pyroxenes can be observed as intermediate compositions between ortho- and clinopyroxene

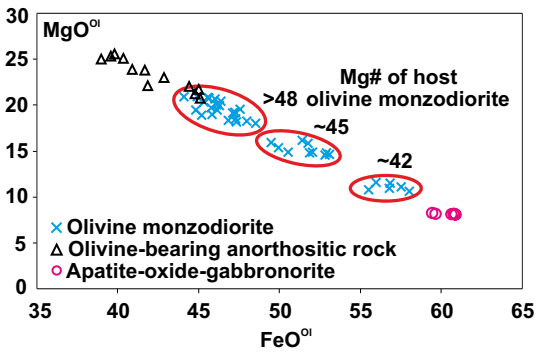

Fig. 7 Olivine MgO versus FeO (in wt%) plot of the Ahvenisto complex olivine monzodiorites, olivine-bearing anorthositic rocks, and apatite–oxide–gabbronorite showing concordant compositional evolution with the whole-rock samples

Fe^{tot} (0.08–0.22) of the samples is in the usual range of mafic rocks. Furthermore, although not in Fe–Mg equilibrium, evolution of the olivine compositions nevertheless seems to correlate with the evolution of the host rock compositions (Figs. 7, 9), which suggests that they are still somehow linked to each other.

All these observations point to the initially counterintuitive conclusion that the apparent mineral-melt disequilibrium could actually be caused by a local equilibrium crystallization process. When magma crystallizes in equilibrium, the bulk Mg/Fe of the magma does not change during crystallization and the resulting whole-rocks preserve the initial Mg#. However, if the crystallizing phases equilibrate with the evolving residual melt, the last possible Mg/Fe recorded by the crystals can be much lower compared to what it would be at liquidus temperatures. In contrast, in

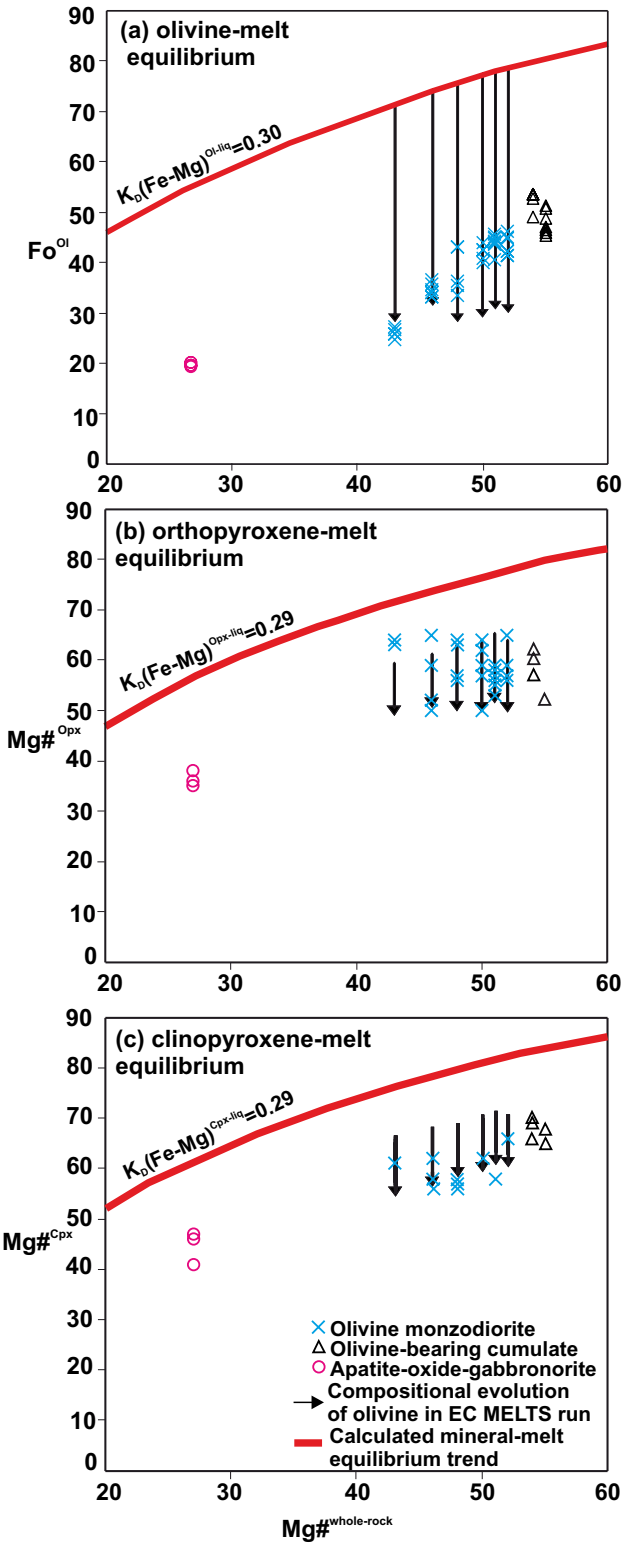

Fig. 9 Measured mineral compositions of the Ahvenisto complex olivine monzodiorites, olivine-bearing anorthositic rocks, and apatite–oxide gabbronorites shown in **a** olivine-melt, **b** orthopyroxene-melt, and **c** clinopyroxene-melt equilibrium diagrams (Roeder and Emslie 1970, see also Putirka 2008) showing the Fe–Mg disequilibrium of the minerals with the measured whole-rock compositions. Black arrows show the range of evolving mineral compositions of modeled olivine–monzodiorites resulting from equilibrium crystallization models conducted with rhyolite-MELTS version 1.2.0 (Gualda et al. 2012). The red line is the calculated mineral-melt equilibrium trend. See text for more details

a fractionally crystallized system, the composition of the melt would evolve and Mg/Fe decrease in the residual melt as crystallizing phases with high Mg/Fe are removed from the system.

In order to test this hypothesis, we used rhyolite-MELTS version 1.2.0 (Gualda et al. 2012) to produce equilibrium crystallization (EC) models for the olivine monzodiorites for which mineral chemical data are available (six samples, Table 1). The models were run in 100 MPa from liquidus temperatures (T_l) determined by MELTS in 5 °C temperature decrement steps with 0.6 wt% of H_2O (Online Resource 1). The models usually yield the mineral assemblage (in the order of crystallization): olivine, plagioclase, spinel, clinopyroxene, apatite, orthopyroxene, oxide, biotite, and alkali feldspar (Table 1). The olivine composition evolves throughout the crystallization model, and the measured olivine compositions are within the range of modeled olivine compositions, except for the most evolved olivine monzodiorite sample (Fig. 9). In the models, pyroxenes begin to crystallize later than olivine, and hence the composition of the remaining melt at that point is already more evolved. Therefore, the Mg# of the first pyroxene to crystallize in the models is already lower than what would be expected if the pyroxene started to crystallize at liquidus temperature. The measured pyroxene compositions are mainly within the range of the model compositions as well (Fig. 9). Note that the rhyolite-MELTS modeling discussed here concentrates on the compositions of the anhydrous Fe–Mg silicates in the most primitive olivine monzodiorites and does not suffer from the same issues of plagioclase stability than the fractional crystallization modeling of more evolved melts discussed in the next section.

Based on these modeling results, we suggest that the apparent Fe–Mg disequilibrium between the mafic minerals and the host olivine monzodiorite whole-rock compositions is the result of equilibrium crystallization. During equilibrium crystallization the forming crystals exchange elements with a continuously evolving melt composition, which in the end results in the minerals being out of equilibrium with the bulk magma system composition. The individual whole-rock samples would thus represent magma batches that crystallized in equilibrium conditions. The process that

Table 1 The Ahvenisto complex olivine monzodiorites used as starting compositions for MELTS models

Starting composition	Process	P (MPa)	T_L (°C)	Order of crystallization	Shown in
RMF-18-249	EC	100	1230.08	Ol, Plg, Spl, Cpx, Ap, Opx, Ox, Bt	Figure 9
RMF-18-255-A	EC	100	1244.53	Ol, Plg, Spl, Cpx, Ap, Opx, Ox, Bt, Kfs	Figure 9
RMF-18-255-B	EC	100	1262.11	Ol, Plg, Spl, Cpx, Ap + Opx, Ox, Bt	Figure 9
RMF-18-258	EC	100	1226.17	Ol, Spl, Plg, Cpx, Ap, Opx, Ox, Bt	Figure 9
RMF-18-259	EC	100	1169.53	Ol, Spl, Plg, Cpx, Ap, Ox, Opx, Bt	Figure 9
RMF-18-260	EC	100	1217.97	Ol, Spl, Plg, Cpx, Ap, Opx, Ox, Bt	Figure 9
APHE-16-6-A	EC	100	1269.14	Ol, Plg, Spl, Cpx, Ap, Opx, Ox, Bt, Kfs	Figure 10
APHE-16-6-A	FC	100	1269.14	Ol, Plg, Spl, Ap, Ox, Cpx, Kfs	Figure 10
APHE-16-6-A	FC	200	1276.56	Ol, Cpx, Plg, Spl, Ap, Ox, Kfs	Figure 10
APHE-16-6-A	FC	400	1290.82	Ol, Opx, Cpx, Plg, Spl, Ap, Ox	Figure 10
APHE-16-6-A	FC	500	1304.3	Opx, Cpx, Plg, Spl, Wtl, Ol, Ap	Figure 10
APHE-16-6-A	FC	600	1322	Opx, Cpx	Figure 10
APHE-16-6-A	FC	700	1339	Opx, Cpx, Wtl, Spl, Plg, Grt, Ap, Ox	Figure 10
APHE-16-6-A	FC	800	1355.66	Opx, Cpx, Wtl, Spl, Grt, Plg, Ap	Figure 10
APHE-16-6-A	FC	900	1371.88	Opx, Cpx, Wtl, Grt, Spl, Plg, Ap, Ox	Figure 10
APHE-16-6-A	FC	1000	1378.5	Opx, Cpx, Wtl, Grt, Spl, Plg, Ap, Ox	Figure 10
APHE-16-6-A	FC	1100	1402.93	Opx, Cpx, Wtl, Grt, Spl, Ap, Plg, Ox	Figure 10
APHE-16-6-A	FC	1200	1417.77	Opx, Cpx, Wtl, Grt	Figure 10

Liquidus temperatures are determined with MELTS and the FC models were run at pressures 100–12,000 MPa (EC only in 100 MPa) in 1-kbar steps with 0.6 wt% of H_2O. Crystallizing phases are listed in the order of crystallization

produced the range of these initial whole-rock compositions is discussed in the following section.

Fractional crystallization of the cumulate rocks and LLDs of the residual melts

While the monzodioritic rocks closely correspond to melt compositions, field relations, petrography, and geochemistry clearly indicate that the olivine-bearing anorthositic rocks and apatite–oxide–gabbronorite are cumulates. They are coarse-grained and contain cumulus plagioclase. The olivine-bearing anorthositic rocks show evidence of plagioclase accumulation by having high amount of plagioclase and high Al_2O_3, CaO, Sr, and Eu and the apatite–oxide–gabbronorite shows evidence of ilmenite and apatite accumulation by having high modal proportions of those minerals and high TiO_2, FeO^{tot}, and P_2O_5 contents (Figs. 2, 3, 4).

On the other hand, the apatite–oxide–gabbronorite shows trace element geochemical characteristics of fairly evolved magma compositions: high total REE, and a strong negative Eu-anomaly (Fig. 5). This might suggest that it represents a rather late-stage cumulate from the monzodioritic series magmas and possibly contains some interstitial melt as well. On the other hand, its REE pattern reflects the REE partition coefficients for apatite (highest for MREE, except for Eu; e.g., Sano et al. 2002), which is found as a cumulus phase. The net effect of accumulation of, for example, apatite and oxides on the major and trace element compositions of the apatite–oxide–gabbronorite sample is difficult to constrain and thus the parental melt composition for this rock type remains uncertain. We suggest that it was more similar to the evolved monzodiorites than olivine monzodiorites, however.

To constrain the possible process producing the cumulates and presumed LLD trend of the monzodioritic rocks (Fig. 10), we utilized two modeling approaches: (1) Rhyolite-MELTS version 1.2.0 (Gualda et al. 2012) was used to conduct thermodynamically constrained fractional crystallization (FC) models for the most primitive olivine monzodiorite composition at varying pressures (100–1200 MPa, 0.6 wt% of H_2O; Table 1). (2) Best-fit parental melt compositions were calculated with MAGFRAC (Morris 1984) software in order to replicate the LLD in two stages using selected monzodioritic compositions as parent and daughter compositions and mineral compositions measured from the anorthositic cumulates (Johanson 1984) as the fractionating phases.

The rhyolite-MELTS FC simulations at 300, 600, and 1200 MPa did not give meaningful results (the software failed to find a solution) and are not considered here further. In Fig. 10, LLDs of the models ran at 100, 400, 700, and 1100 MPa are shown. This set of models illustrates the effect of increasing pressure adequately and the other successful runs plot within or very close to a field bordered by them. None of the simulations show very good fit with the data, but the ones run at lower pressures (especially the simulation at 100 MPa) are better.

For input parameters of the MAGFRAC (Morris 1984) model, we selected a two-stage approach based on major changes in the modal and geochemical composition between the olivine monzodiorites and monzodiorites. The division of the stages was set at Mg# of ~ 40 because rocks more primitive than that contain olivine and lack amphibole and have no or negligible negative Eu-anomaly, whereas rocks with Mg# < 40 lack olivine but contain amphibole and exhibit a negative Eu-anomaly. We selected the most primitive olivine monzodiorite as Parent 1, one of the intermediate monzodiorites as Parent 2 and Daughter 1, and one of the most evolved monzodiorites as Daughter 2. Representative analyses of plagioclase, pyroxenes, olivine, and ilmenite from the anorthositic rocks (Johanson 1984) were used as the compositions of the fractionating phases (Table 2). The estimated parent compositions are very close fits to the parent compositions used in the calculations and model gives very reasonable r^2 values of 0.284 for stage 1 and 0.375 for stage 2 (Table 2; Fig. 10). A fractionation trend from the estimated parent to daughter is plotted in Fig. 10.

The major problem in the MELTS models is the delayed crystallization of plagioclase, which has also been observed to be an issue in some other occasions (see Putirka 2005). Petrographic observations indicate that plagioclase is the first phase to crystallize, but in the models plagioclase starts to crystallize only after the magma temperature has decreased 165 °C causing delayed depletion of Al_2O_3 in the residual melt. Neither MELTS nor rhyolite-MELTS are well suited for igneous systems with intermediate composition and phase assemblage dominated by amphibole and biotite (Ghiorso and Sack 1995; Gualda et al. 2012). Both amphibole and biotite are major phases in the monzodiorites (but not in olivine monzodiorites, cf. previous section), which might also play a role in the mismatch between the rhyolite-MELTS fractionation models and the observations. The strength of the MAGFRAC modeling lies in the fact that it is based on actual observed mineral parageneses and measured mineral compositions. The MAGFRAC model also supports the assumption that the poor fit of the rhyolite-MELTS models in Al_2O_3 and CaO is due to the inability of MELTS to correctly stabilize plagioclase in the modeled compositions.

The close fit of the MAGFRAC models to the observations, thus, strongly supports the hypothesis that the compositions of the monzodioritic magmas evolved in a fractionally crystallizing system that produced the juxtaposed anorthositic cumulates and that the monzodiorites represent their residual liquids. Individual monzodiorite magma batches were then intermittently tapped from this evolving reservoir and crystallized in equilibrium conditions as described in the previous section.

Implications for the petrogenesis of the Ahvenisto complex and Fennoscandian rapakivi magmatism

The Ahvenisto complex belongs to the Fennoscandian rapakivi magmatic system (Rämö and Haapala 2005) which spans a time interval of over 100 my (1.65–1.52 Ga; Rämö et al. 2014). Most likely the complex represents a volumetrically small but early (ca. 1.64 Ga; Heinonen et al. 2010b) series of compositionally diverse magma pulses related to the Wiborg magma system (Heinonen et al. 2016, 2017) and intruded and crystallized in a shallow (1–5 km) upper crustal magma chamber. Compositionally, the rock types of the complex represent the complete AMCG array observed in the Wiborg magma system and present a unique setting to study the magmatic emplacement and crystallization history of the entire rapakivi suite from its lower crustal origins all the way to the final emplacement at upper crustal levels.

Orthopyroxene megacrysts (HAOM) and associated megacrystic plagioclase entrapped within massif-type anorthosite cumulates have been interpreted to represent the earliest, deep stage of crystallization in anorthosite massifs (e.g., Heinonen et al. 2020 and references therein). It has been suggested that the megacrysts with the highest Al_2O_3 contents crystallized at high pressures from mantle-derived high-Al tholeiitic melts, which are presumed parental to massif-type anorthosites (e.g., Emslie et al. 1994; Charlier et al. 2010). Their isotope compositions also suggest that crustal assimilation occurred before plagioclase accumulation (Bybee et al. 2015). The accumulation of buoyant plagioclase enabled the ascent of the anorthositic crystal mushes through the crust leaving denser mafic cumulates behind (e.g., Bybee et al. 2019). Some HAOMs were carried to shallower crustal levels by the ascending mushes and record mineralogical evidence of low-pressure re-equilibration (e.g., exsolved plagioclase lamellae; Emslie 1975). The compositional zoning of HAOMS suggest that continuous crystallization took place during ascent and composition of the matrix orthopyroxene in the host anorthositic rocks indicates that final crystallization happened at upper crustal levels (Heinonen et al. 2020). The continuous crystallization of plagioclase and mafic phases from the mushes left behind a residual magma, usually considered to be monzodioritic in composition (e.g., Emslie et al. 1994; Markl and Frost 1999; Markl 2001; Heinonen et al. 2010b; Charlier et al. 2010). Observations of HAOMs and Al-in-opx geobarometry suggest similar polybaric crystallization history for the Ahvenisto anorthosites and for the entire Wiborg magma system (Heinonen et al. 2020).

Based on the evidence presented above and the polybaric crystallization hypothesis (Heinonen et al. 2020), we interpret that the monzodioritic rocks of the Ahvenisto complex represent such residual melts after fractional crystallization of anorthositic cumulates in a shallow (< 200 MPa) magma

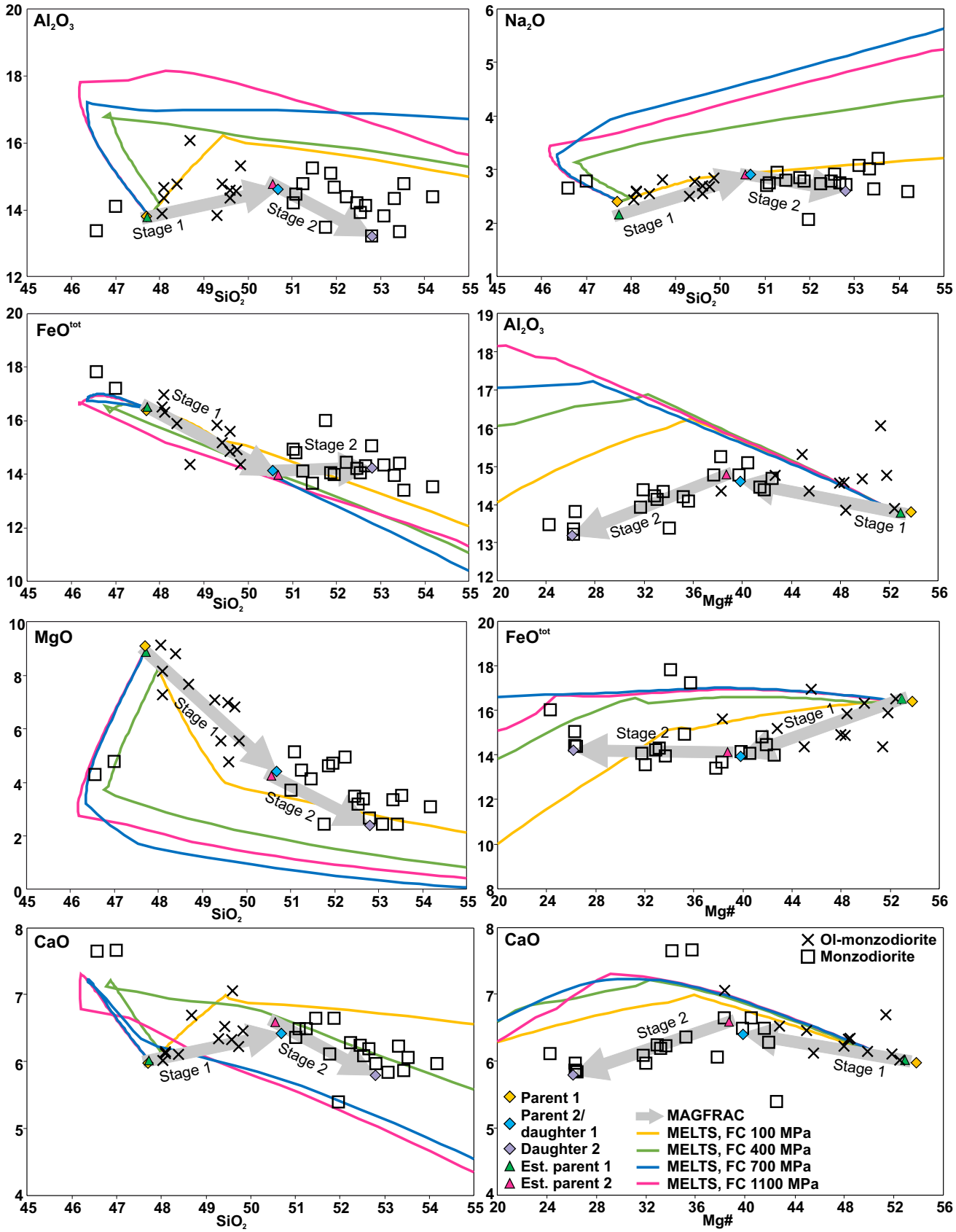
Al2O3
Na2O
FeOtot
Al2O3
MgO
FeOtot
CaO
CaO
SiO2
Mg#
Stage 1
Stage 2
Ol-monzodiorite
Monzodiorite
Parent 1
Parent 2/ daughter 1
Daughter 2
Est. parent 1
Est. parent 2
MAGFRAC
MELTS, FC 100 MPa
MELTS, FC 400 MPa
MELTS, FC 700 MPa
MELTS, FC 1100 MPa

◂**Fig. 10** Selected variation diagrams showing the modeled melt compositions and results of crystallization modeling (rhyolite-MELTS, MAGFRAC) plotted with the monzodioritic rocks of the Ahvenisto complex. Only LLDs of rhyolite-MELTS runs at 100, 400, 700, and 1100 MPa for FC and 100 MPa for EC (Table 1) are shown. Gray arrows present the LLDs between estimated parent and daughter magmas of the MAGFRAC models in two stages (Table 2): the estimated parents plot close to the used parent compositions and the stages give r^2 values of 0.284 (Stage 1) and 0.375 (Stage 2). Only samples of this study are shown for clarity

chamber, i.e. during the latest stages in the overall crystallization history of the complex. The monzodioritic residual melt moved towards more evolved compositions (lower Mg#:s) due to continuous fractionation of plagioclase (+ olivine + pyroxene + oxide), which formed the anorthositic cumulates. Batches of the monzodioritic residual melts were extracted from the fractionating system and crystallized in equilibrium producing the observed mineral assemblage characterized by low-Mg# mafic phases (Fig. 9). This interpretation lends further support to the previous models (Fred et al. 2019) in which interaction (mixing or mingling) between granitic and monzodioritic magmas observed in the Ahvenisto complex were suggested to have been controlled by the continuous extraction of compositionally evolving monzodioritic material to shallower crustal levels. During the ultimate shallow-level fractionation stages, accumulation of oxide, apatite, Fe- rich mafic phases, and An-poor plagioclase led to the formation of the apatite–oxide–gabbronorite.

The melts that the Ahvenisto complex rocks crystallized from had already gone through prior differentiation and assimilation, which is recorded in the isotopic signature of the whole complex (Heinonen et al. 2010b, 2015). Based on the relatively shallow erosional level in Fennoscandia and seismic studies (Luosto et al. 1990; Elo and Korja 1993), a presumption that the main anorthositic mass most likely still remains unexposed at mid-crustal levels has been made (see Rämö and Haapala 1996). The rock types observed in Ahvenisto indicate that this mid-crustal mass may contain larger amounts of anorthositic cumulates and their Fe–Ti–P-rich residual liquids crystallized at deeper levels. Consequently, although the Ahvenisto complex is only a small upper crustal level intrusion, it can be used to study the processes that have affected the formation of AMCG assemblages even in larger suites consisting of several intrusions, such as the Nain Plutonic Suite in Labrador, Canada.

Significance of monzodioritic rocks in AMCG petrogenesis—a global comparison

Major element compositions of monzodiorites and OAGNs globally are plotted in Fig. 11 to compare them with the data and models (MAGFRAC and MELTS FC, 100 MPa) of this study. The samples of all rock types show wide variation in composition and the global monzodioritic group overlaps with some of the OAGNs (Fig. 11). This overlap may reflect not only the differing classification of these Fe–Ti–P-rich rocks in various studies but also gradation from melt-representative samples to cumulus-dominated samples.

Monzodioritic rocks

Most of the monzodioritic rocks from other AMCG suites show similar major element characteristic to the Ahvenisto monzodioritic rocks and form a trend similar to what we suggest to represent the LLD of anorthosite residual melt evolution. However, the Ahvenisto olivine monzodiorites seem to define a compositionally unique group and almost no monzodioritic rocks with such high Mg-contents have been reported in any other AMCG suite. Although the general monzodioritic trend is similar, overall the Ahvenisto monzodioritic rocks have lower CaO and marginally lower Na_2O and P_2O_5 content than those from most other suites.

There seems to be two trends in terms of SiO_2 vs. MgO: some of the monzodioritic rocks plot on similar high MgO trend with the Ahvenisto olivine monzodiorites and others diverge towards the OAGNs (Fig. 11c). The former trend may represent a melt-evolution trend and the latter an accumulation trend. Similar, but less clearly distinguishable branching trends are present in the SiO_2 vs. TiO_2 and P_2O_5 plots (Fig. 11a, g). In general, the monzodioritic rocks from other suites having similar Mg# with the Ahvenisto olivine monzodiorites have elevated Al_2O_3 and CaO similar to Ahvenisto olivine-bearing anorthositic rocks (Fig. 11b, f), however, indicating they are more likely cumulates than melt compositions. The relatively lower Ca, Na, and P of the Ahvenisto rocks, compared to other monzodioritic rocks, indicates that there were differences in the contents of these elements in the parental melts (or in the possible assimilated material) between the different suites (see Duchesne 1990; Bybee et al. 2015), regardless of the general fractionation trends being similar. In addition, the mode of fractionated material, that depended not only on composition but also on the prevailing P–T conditions, may have had an effect on the residual liquid trends.

Despite the apparent compositional differences between the localities, the LLD models constructed in this study indeed fit the observed global trends rather well (Fig. 11). With local adjustments of the input parameters, our models could be applicable also to other AMCG suites. Only the olivine monzodiorites are somewhat deviant from the general trends of monzodioritic rocks from other suites. However, this comparison is hampered by the general rarity of such primitive compositions and inclusion of cumulate rocks (rocks comparable to the Ahvenisto olivine-bearing anorthositic rocks and OAGNs, which will be discussed below) within the monzodioritic rock group elsewhere.

Table 2 Parent, daughter, and phase compositions used in MAGFRAC calculations (Morris 1984) together with estimated parent compositions and r^2 values

Stage 1	Parent 1	Est. Parent	Daughter 1	ol	plg	cpx	opx
SiO_2	47.70	47.72	50.68	35.60	53.35	51.86	50.71
TiO_2	1.60	1.43	2.66	0.00	0.07	0.97	0.16
Al_2O_3	13.80	13.78	14.61	0.00	30.54	2.77	0.74
FeO*	16.38	16.52	13.93	38.65	0.55	11.66	25.40
MnO	0.21	0.21	0.18	0.45	0.00	0.03	0.49
MgO	9.09	8.86	4.40	26.95	0.04	13.50	20.23
CaO	5.98	6.01	6.42	0.00	12.51	20.52	1.34
Na_2O	2.40	2.15	2.90	0.00	3.14	0.30	0.02
K_2O	1.45	1.11	2.02	0.00	0.24	0.01	0.00
P_2O_5	0.47	0.44	0.84	0.00	0.00	0.00	0.00
Total	99.08	98.23	98.63	101.65	100.44	99.60	99.67
Proportion			51.93	18.82	19.80	0.33	7.35
Sum r^2	0.284						

Stage 2	Parent 2	Est. Parent	Daughter 2	opx	plg	cpx	ol	ilm
SiO_2	50.68	50.56	52.80	50.08	55.48	49.06	35.60	0.00
TiO_2	2.66	2.42	2.60	0.12	0.09	0.29	0.00	46.32
Al_2O_3	14.61	14.78	13.20	0.56	29.72	1.19	0.00	0.01
FeO*	13.93	14.14	14.22	35.35	0.50	23.88	38.65	53.03
MnO	0.18	0.20	0.20	0.62	0.00	0.52	0.45	1.12
MgO	4.40	4.26	2.40	12.40	0.02	11.20	26.95	0.01
CaO	6.42	6.59	5.80	2.45	9.91	14.59	0.00	0.00
Na_2O	2.90	2.90	2.59	0.03	5.87	0.11	0.00	0.00
K_2O	2.02	2.42	3.68	0.00	0.30	0.00	0.00	0.00
P_2O_5	0.84	0.68	1.06	0.00	0.00	0.00	0.00	0.00
Total	98.63	98.95	98.55	101.61	101.89	100.84	101.65	100.49
Proportion			63.10	−1.40	21.48	5.66	8.54	1.57
Sum r^2	0.375							

Parent and daughter compositions are Ahvenisto complex monzodioritic rocks and phase compositions are from Ahvenisto complex anorthositic cumulates (Johanson 1984)

Oxide–apatite–gabbroborites

Although some of the OAGNs show similar major element characteristics with the monzodiorites, majority of the OAGN samples define scattered compositional arrays and show clearly distinct features, which are not compatible with residual liquid origins. Compared to the monzodioritic rocks, OAGNs have higher TiO_2, FeO^{tot}, MgO, CaO, and P_2O_5 and lower SiO_2, Al_2O_3, Na_2O, and K_2O due to strong accumulation of mafic minerals (pyroxenes ± olivine), oxide, and apatite (Figs. 4, 11).

Although the OAGNs show cumulus characteristics, they are very different from the anorthositic cumulates that have formed by the accumulation of plagioclase (Fig. 11). The composition of the OAGNs and their spatial relations suggest that they are also genetically associated with the monzodioritic rocks, however, and thus most likely still crystalized and accumulated from the same magmatic lineage as the anorthositic cumulates. Although the one sample from Ahvenisto suggests that it has formed during late stages in the evolution of the complex, the global data tentatively suggest that the OAGNs are formed throughout the crystallization history of anorthosites (see also Dymek and Owens 2001). Although OAGNs and monzodioritic rocks appear consanguineous, our modeling and observations suggest that the OAGNs, which are of cumulate origin, should not be grouped together with the melt-representative monzodioritic rocks.

Alternative modes of origin for the monzodioritic rocks in AMCG suites

We are not the first to propose a residual liquid origin for monzodioritic rocks in AMCG complexes. For example, Bybee et al. (2015) suggested that fractionation of olivine-bearing anorthositic rocks would leave behind Fe-, apatite-,

and oxide-enriched residual melts with OAGN affinities and the anorthositic fractionation without olivine would produce SiO_2-enriched residuals with monzodioritic compositions.

Although many of the studies on monzodioritic rocks in AMCG complexes argue for their residual liquid nature (e.g., Ashwal 1982; Morse 1982; Duchesne 1984; Owens and Dymek 1992; McLelland et al. 1994; Mitchell et al. 1996; Vander Auwera et al. 1998; Dymek and Owens 2001; Markl 2001; Heinonen et al. 2010b), some fundamentally different models for their origin have also been suggested. One of them suggest that the monzodioritic rocks would represent the actual parental magmas of the anorthositic rocks, like in studies of the Hidra massif of the Neoproterozoic Rogaland anorthosite province in SW Norway (e.g., Duchesne et al. 1974; Duchesne and Demaiffe 1978; Demaiffe and Hertogen 1981). Based on trace element fractional crystallization models, major element mass balance calculations, trapped liquid compositions, and lack of mafic veins, the charnokitic rocks associated with the anorthosites have, instead of monzodiorites, been inferred to represent residual liquids (Demaiffe and Hertogen 1981). One of the key arguments for the parental nature of monzodioritic rocks has been the lack of a negative Eu-anomaly that would had inevitably been produced by extensive plagioclase fractionation, especially in the reducing conditions characteristics of AMCG magmatism. However, this generalization is somewhat thwarted by the early saturation of apatite in the monzodioritic magmas, which drastically affects the bulk partition coefficients between minerals and melts and their ability to enrich REEs (Watson 1979). Fractionation of apatite has the opposite effect to Eu relative to that of plagioclase in reducing conditions and, therefore, may lead to smaller or lack of negative Eu-anomalies in the monzodioritic rocks as also observed in the monzodioritic rocks of this study.

A relatively early study on anorthositic suites suggested that monzodioritic rocks would represent intermediate derivatives of magmas parental to the entire AMCG series (De Waard and Romey 1969). Regardless of the suggested parental magma composition and source, many studies have since then described the bimodal (mafic-felsic) origin of AMCG rock types (e.g., Emslie et al. 1994; Ashwal and Bybee 2017 and reference therein). In addition, in order to produce the large amounts of more evolved compositions from the monzodioritic melts, very high degree of fractionation and considerably larger amounts of monzodioritic melts would be required than what are observed in most AMCG suites (e.g., Kolker et al. 1991). Especially, this mode of origin is not viable in the granite-dominated AMCG localities such as the Wiborg rapakivi suite.

On the other hand, the low Cr content and peculiar Sr-isotope composition of some monzodioritic rocks has led to suggestions that the monzodiorites are coeval but not comagmatic with the anorthosites (e.g., Emslie 1978; Duchesne et al. 1989; Duchesne 1990). The Sr content of some monzodioritic rocks have been interpreted as evidence of origin from basic crustal melts (e.g., Emslie 1978; Duchesne et al. 1989, 2017). Such low-degree melts would be enriched in Fe, Ti, and P and have lower SiO_2 compared to starting material, and their composition would be similar to those of the monzodiorites.

Based on observed textures and experimental work an immiscible liquid origin for the monzodiorites have been suggested as well (e.g., Philpotts 1981; Powell et al. 1982). Crystallization of plagioclase from basaltic to andesitic magma leads to immiscible silica-rich and Fe-rich liquids (e.g., Philpotts 1981; Powell et al. 1982) and continued fractionation of plagioclase from these liquids would result in magneritic and monzodioritic composition, respectively. Further fractionation of the Fe-rich melt would lead to accumulation of oxides and apatite (Philpotts 1981).

The Nd–Sr-isotope compositions of the Ahvenisto complex anorthositic rocks (ε_{Nd} −0.9 to −0.5, Sr_i 0.7037 to 0.7041) and monzodioritic rocks (ε_{Nd} −1.1 to −0.2, Sr_i 0.7028 to 0.7040) overlap suggesting a comagmatic relationship at least in their case (Heinonen et al. 2010b). Furthermore, Hf–O isotopes suggest a mantle origin for these rocks, while the granitic rocks of the suite show a clearly separate crustal signature (Heinonen et al. 2010a, 2015). Thus, the isotopic evidence rules out the possibility that the Ahvenisto monzodioritic rocks could be intermediate derivatives between anorthositic and granitic rocks or that they would be consanguineous with the granitic rocks in any other way. Immiscibility into two contrasting liquid compositions (i.e. monzodioritic vs. granitic lineages) prior to their late-stage independent fractionation is also unlikely based on the isotopic evidence of the Ahvenisto rocks.

We tentatively suggest, based on our observations, that the most suitable global mode of origin for the monzodioritic rocks is that they represent residual melt compositions after anorthosite fractionation and that with some modification the fractional crystallization models outlined in this study could be applied to other AMCG suites as well. The equilibrium crystallization stage revealed by a detailed mineral chemical analysis that followed the main fractionation stage in Ahvenisto requires further verification from other AMCG localities. The olivine monzodiorites are the most primitive melts in Ahvenisto, and although scarcely found in other AMCG suites, have potential to serve to help to trace the origin and ultimate parental melts of massif-type anorthosites.

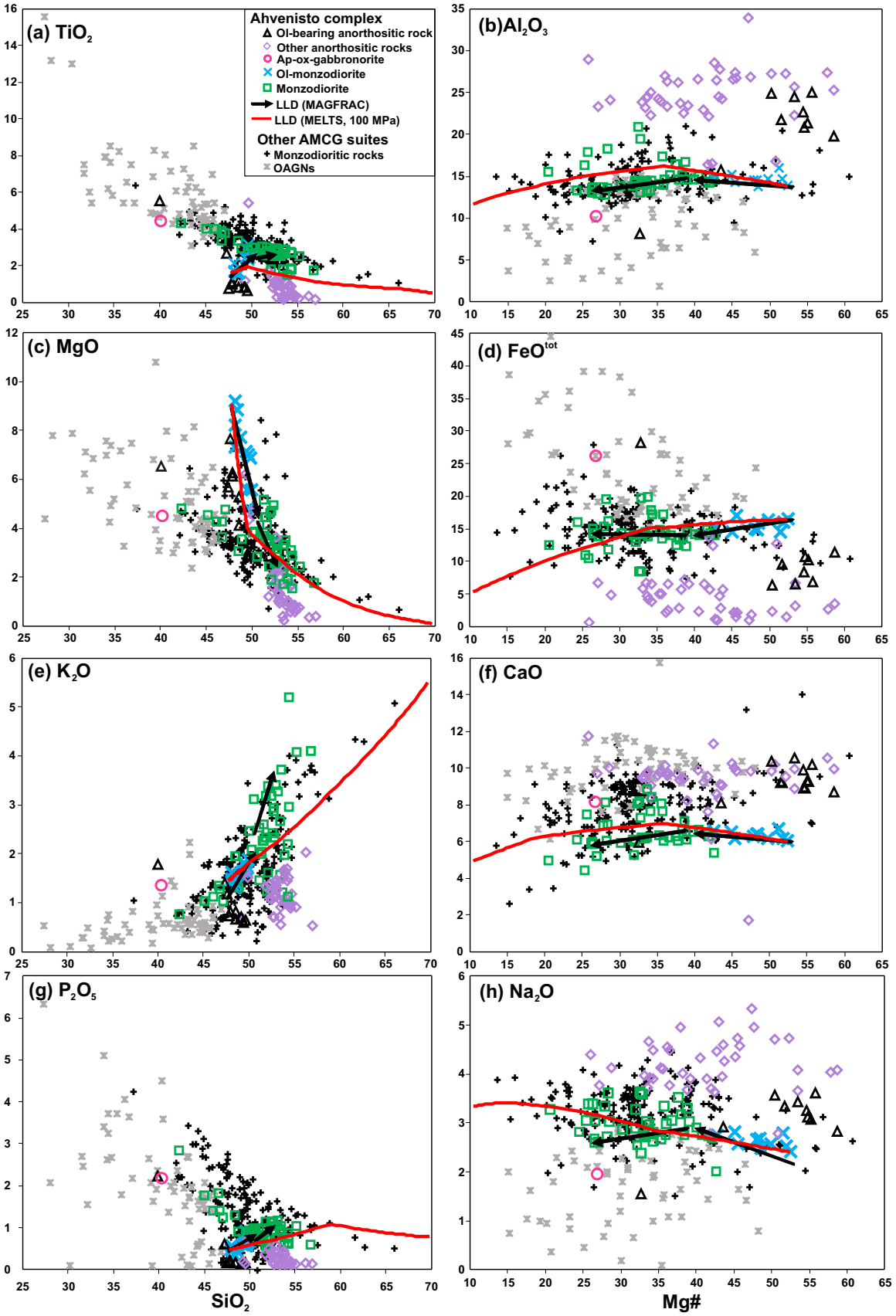
(a) TiO2
(b)Al2O3
(c) MgO
(d) FeOtot
(e) K2O
(f) CaO
(g) P2O5
(h) Na2O
Ahvenisto complex
Ol-bearing anorthositic rock
Other anorthositic rocks
Ap-ox-gabbronorite
Ol-monzodiorite
Monzodiorite
LLD (MAGFRAC)
LLD (MELTS, 100 MPa)
Other AMCG suites
Monzodioritic rocks
OAGNs
SiO2
Mg#

◂**Fig. 11** Major element variations of the Ahvenisto complex monzodioritic rocks, olivine-bearing anorthositic rocks, and apatite–oxide–gabbronorite (this study; Johanson 1984; Heinonen et al. 2010a, b) and the presented LLD models (MAGFRAC and rhyolite-MELTS FC at 100 MPa; Tables 1, 2) compared to a global compilation of monzodiorite and OAGN data from other AMCG suites. Locations and data sources for the monzodiorite data are the following: Hidra and Eia-Rekelfjord, Norway (Duchesne et al. 1974); Labrador and Grenville, Canada and SW Norway (Emslie 1978 and reference there in); Hidra, Norway (Demaiffe and Hertogen 1981); Egersund-Ogna, Norway (Duchesne et al. 1985); Morin, St. Urbain, and Labrieville, Canada (Owens et al. 1993); Nain, Canada (Emslie et al. 1994); Laramie, USA (Mitchell et al. 1996); Rogaland, Norway (Vander Auwera et al. 1998); Adirondacks, USA (Seifert et al. 2010); and Korosten, Ukraine (Duchesne et al. 2017). Locations and data sources for the OAGN data are: Saririaky, Madagascar (Ashwal et al. 1998); Laramie, USA (Mitchell et al. 1996); Château-Richer, St. Urbain, and Labrieville, Canada and Roseland and Carthage; USA (Dymek and Owens 2001); Adirondacks, USA (Seifert et al. 2010)

Conclusions

The monzodioritic rocks and apatite–oxide–gabbronorite in the Ahvenisto AMCG complex, southeastern Finland, represent residual compositions left after fractional crystallization and formation of the anorthositic cumulate rocks. The monzodioritic rocks are fine-grained, show no cumulus features, are enriched in REE compared to the anorthositic rocks, and seem to form an LLD trend that can be reproduced by petrological modeling using observed whole-rock and mineral compositions. Instead, the apatite–oxide–gabbronorite has relatively lower low SiO_2, but higher FeO^{tot}, TiO_2, and P_2O_5 and has formed by accumulation from more evolved monzodioritic magmas.

We suggest that the variety of different anorthositic and monzodioritic rock types is controlled by fractional crystallization of plagioclase and mafic minerals in a shallow magma chamber during the late evolutionary stages of the Ahvenisto magma system. Subsequent equilibrium crystallization of such differentiated magma batches explains the mineral composition and the low Mg# of olivine and pyroxenes in individual samples.

We suggest that the presented models, with modified suite-specific constraints, could be applicable to other AMCG suites as well.

Acknowledgements We thank the Doctoral Programme in Geoscieces (GEODOC), K.H. Renlunds Foundation, and Academy of Finland (Grant 295129) for funding this research. The help of Radoslaw Michallik with sample preparation and EMPA analysis, valuable comments by reviewers Carol Frost and Grant Bybee, and efficient editorial handling by Mark Ghiorso are gratefully acknowledged.

Funding Open access funding provided by University of Helsinki including Helsinki University Central Hospital.

References

Alviola R, Johanson BS, Rämö OT, Vaasjoki M (1999) The Proterozoic Ahvenisto rapakivi granite-massif-type anorthosite complex, southeastern Finland; petrography and U-Pb chronology. Precambrian Res 95:89–107

Ashwal LD (1982) Mineralogy of mafic and Fe-Ti oxide-rich differentiates of the Marcy anorthosite massif, Adirondack, New York. Am Mineral 67:14–27

Ashwal LD (1993) Anorthosites. Springer, Berlin, p 422

Ashwal LD (2010) The temporality of anorthosites. Can Mineral 48:711–728

Ashwal LD, Bybee GM (2017) Crustal evolution and the temporality of anorthosites. Earth Sci Rev 173:307–330

Ashwal LD, Twist D (1994) The Kunene complex, Angola/Namibia: a composite anorthosite massif-type anorthosite complex. Geol Mag 131:579–591

Ashwal LD, Hamilton MA, Morel VPI, Rambeloson RA (1998) Geology, petrology and isotope geochemistry of massif-type anorthodites from southwest Madagascar. Contrib Mineral Petrol 133:389–401

Boynton WV (1984) Geochemistry of rare earth elements: meteorite studies. In: Henderson P (ed) Rare earth element geochemistry. Elsevier, Amsterdam, pp 63–114

Bryan WB, Finger LW, Chayes F (1969) Estimating proportions in petrographic mixing equations by least-squares approximation. Science 163:926–927

Bybee GM, Ashwal LD (2015) Isotopic disequilibrium and lower crustal contamination in slowly ascending magmas: insights from Proterozoic anorthosites. Geochim Cosmochim Acta 167:286–300

Bybee GM, Ashwal LD, Gover CF, Hamilton MA (2015) Pegmatitic pods in the Mealy Mountains Intrusive Suite, Canada: clues to the origin of the olivine-orthopyroxene dichtomy in Proterozoic anorthosites. J Petrol 56:845–868

Bybee GM, Hayes B, Owen-Smith TM, Lehmann J, Ashwal LD, Brower AM, Hill CM, Corfu F, Manga M (2019) Proterozoic massif-type anorthosites as the archetypes of long-lived (>100 Myr) magmatic systems—new evidence from the Kunene Anorthosite complex (Angola). Precambr Res 332:1–16

Charlier B, Duchesne JC, Vander Auwera J, Storme JY, Maquil R, Longhi J (2010) Polybaric fractional crystallization of high-alumina basalt parental magmas in the Egersund-Ogna massif-type aorthosite (Rogaland, SW Norway) constrained by plagioclase and high-alumina orthopyroxene megacrysts. J Petrol 51(12):2515–2546

De Waard D, Romey WD (1969) Chemical and petrologic trends in the anorthosite-charnokite series of the snowy mountain massif, Adirondack highlands. Am Minreal 54:529–538

Demaiffe D, Hertogen J (1981) Rare-earth element geochemistry and strontium isotopic composition of a massif-type anorthositic-charnokitic body: the Hidra Massif (Rogaland, SW Norway). Geochem Cosmochim Acta 45:1545–1561

Duchesne JC (1984) Massif anorthosites: another partisan review. Feldspars Felspathoids C137:411–433

Duchesne JC (1990) Origin and evolution of monzonorites related to anorthosites. Schweizerische Mineralogishe und Petrographische Mitteilungen 70:189–198

Duchesne JC, Demaiffe D (1978) Trace elements and anorthosite genesis. Earth Planet Sci Lett 38:249–272

Duchesne JC, Roelandts I, Demaiffe D, Hertogen J, Gibjels R, De Winter J (1974) Rare-earth data on monzonoritic rocks related to anorthosites and their bearing on the nature of the parental magma of the anorthositic series. Earth Planet Sci Lett 24:325–335

Duchesne JC, Roelandts I, Demaiffe D, Weis D (1985) Petrogenesis of monzonoritic dykes in the Egersund-Ogna anorthosite (Rogaland, S.W. Norway): trace elements and isotopic (Sr, Pb) constraints. Contrib Mineral Petrol 90:214–225

Duchesne JC, Wilmart E, Demaiffe D, Hertogen J (1989) Monzonorites from Rogaland (Southwest Norway): a series of rocks coeval but not comagmatic with massif-type anorthosites. Precambrian Res 45:111–128

Duchesne JC, Liégeois JP, Vander Auwera J, Longhi J (1999) The crustal tongue melting model and the origin of massif anorthosites. Terra Nova 11:100–105

Duchesne JC, Shumlyanskyy L, Mytrokhyn OV (2017) The jotunite of the Korosten AMCG complex (Ukranian shield): crust- or mantle-derived? Precambrian Res 299:58–74

Dymek RF, Owens BE (2001) Petrogenesis of apatite-rich rocks (nelsonites and oxide-apatite gabbronorites) associated with massif anorthosites. Econ Geol 96:797–815

Eklund O (1993) Coeval contrasting magmatism and magma mixing in proterozoic post- and anorogenic granites, Åland, SW Finland. Ph.D. Thesis, Åbo University, p 58

Elo S, Korja A (1993) Geophysical interpretation of the crustal and the upper mantle structure in the Wiborg rapakivi granite area, southeastern Finland. Precambrian Res 64:273–288

Emslie RF (1975) Pyroxene megacrysts from anorthositic rocks: new clues to the sources and evolution of the parent magmas. Can Mineral 13:138–145

Emslie RF (1978) Anorthosite massifs, rapakivi granites, and late Proterozoic rifting of North America. Precambrian Res 64:273–288

Emslie RF, Hamilton MA, Thériault RJ (1994) Petrogenesis of a Mid-Proterozoic anorthosite-mangerite-charnockite-granite (AMCG) complex: isotope and geochemical evidence from the Nain Plutonic suite. J Geol 102:539–558

Fred R, Heinonen A, Heikkilä P (2019) Tracing the styles of mafic-felsic magma interaction: a case study from the Ahvenisto igneous complex, Finland. Bull Geol Soc Finl 91:5–33

Frost CD, Frost BR (1997) Reduced rapakivi-type granites: the tholeiite connection. Geology 25:647–650

Ghiorso MS, Sack RO (1995) Chemical mass transfer in magmatic processes IV. A revised and internally consistent thermodynamic model for the interpolation and extrapolation of liquid-solid equilibria in magmatic systems at elevated temperatures and pressures. Contrib Mineral Petrol 119:197–212

Ghiorso MS, Gualda GAR (2015) An H_2O–CO_2 mixed fluid saturation model compatible with rhyolite-MELTS. Contrib Mineral Petrol 169:53. https://doi.org/10.1007/s00410-015-1141-8

Gualda GA, Ghiorso MS, Lemons RV, Carley TL (2012) Rhyolite-MELTS: a modified calibration of MELTS optimized for silica-rich, fluid-bearing magmatic systems. J Petrol 53:875–890

Hargreaves JC (2015) Summary of quality control data for the geoscience laboratories methods CTK-100, SGT-R01, IMP-200, XRF-M01, XRF-M02, XRF-T02 and XRF-T03. In: Summary of field work and other activities 2015, Ontario Geological Survey, Open File Report 6313, pp 39–1 to 39–11

Hargreaves JC (2017) Summary of quality control data for the geoscience laboratories methods EMP-100, IMC-100, IMO-100 and ISE-R01. In: Summary of field work and other activities, 2017, Ontario Geological Survey, Open File Report 6333, pp 32–1 to 32–15

Hargreaves JC (2019) Summary of quality-control data for the geoscience laboratories methods FEO-ION, IAW-200, ICW-100, IRC-100, IRW-H2O and TOC-100. In: Summary of field work and other activities, 2019, Ontario Geological Survey, Open File Report 6360, pp 25–1 to 25–6

Heinonen A (2012) Isotopic evidence for the origin of Proterozoic massif-type anorthosites and their relation to rapakivi granites in southern Finland and northern Brazil. Department of Geosciences and Geography, A18. Helsinki. Unigrafia

Heinonen A, Andersen T, Rämö OT (2010a) Re-evaluation of rapakivi petrogenesis: source constraints from the Hf isotope composition of zircon in the rapakivi granites and associated mafic rocks of southern Finland. J Petrol 51:1687–1709

Heinonen A, Rämö OT, Mänttäri I, Johanson B, Alviola R (2010b) Formation and fractionation of High-Al tholeiitic magmas in the Ahvenisto rapakivi granite–massif-type anorthosite complex, southeastern Finland. Can Mineral 48:969–990

Heinonen A, Andersen T, Rämö OT, Whitehouse MJ (2015) The source of Proterozoic anorthosite and rapakivi granite magmatism: evidence from combined in situ Hf-O isotopes of zircon in the Ahvenisto complex, southeastern Finland. J Geol Soc 172:103–112

Heinonen A, Mänttäri I, Rämö OT, Andersen T, Larjamo K (2016) A priori evidence for zircon antecryst entrainment in megacrystic Proterozoic granites. Geology 44:227–230

Heinonen A, Mänttäri I, Rämö OT, Andersen T, Larjamo K (2017) Zircon as a proxy for the magmatic evolution of Proterozoic ferroan granites; the Wiborg rapakivi granite batholith, SE Finland. J Petrol 58:2493–2517

Heinonen A, Kivisaari H, Michallik RM (2020) High-aluminum orthopyroxene megacrysts (HAOM) in the Ahvenisto complex, SE Finland, and the polybaric crystallization of massif-type anorthosites. Contrib Mineral Petrol 175:1–25

Johanson BS (1984) Ahvenisto gabbro-anortosit komplex- En petrografisk och mineralogisk undersökning. Helsingfors universitet, Helsinki

Kolker A, Frost CD, Hanson GN, Geist DJ (1991) Neodymium, strontium, and lead isotopes in the Maloin Ranch Pluton, Wyoming: Implications for the origin of evolved rocks at anorthosite margins. Geochem Cosmochim Acta 55:2285–2297

Maitre Le et al (2002) Igneous rocks: a classification and glossary of terms. Cambridge University Press, Cambridge

Luosto U, Tiira T, Korhonen H, Azbel I, Burmin V, Buyanov A, Kosminskaya I, Ionkis V, Sharov N (1990) Crust and upper mantle structure along the DSS Baltic profile in SE Finland. Geophys J Int 101:89–110

Markl G (2001) REE constraints on fractionation processes of massif-type anorthosites on the Lofoten Islands, Norway. Mineral Petrol 72:325–351

Markl G, Frost BR (1999) The origin of anorthosites and related rocks from the Lofoten Island, Northern Norway. II. Modelling of parental melts for anorthosites. J Petrol 40:61–77

McLelland J, Ashwal L, Moore L (1994) Composition and petrogenesis of oxide-, apatite-rich gabbronorites associated with Proterozoic anorthosite massifs: examples from the Adirondack Mountains, New York. Contrib Mineral Petrol 116:225–238

Michallik RM, Wagner T, Fusswinkel T, Heinonen JS, Heikkilä P (2017) Chemical evolution and origin of the Luumäki gem beryl

pegmatite: constraints from mineral trace element chemistry and fractionation modeling. Lithos 274–275:147–168
Mitchell JN, Scoates JS, Frost CD (1995) High-Al gabbros in the Laramie Anorthosite Complex, Wyoming: implications for the composition of melts parental to Proterozoic anorthosite. Contrib Mineral Petrol 119:166–180
Mitchell JN, Scoates JS, Frost CD, Kolker A (1996) The geochemical evolution of anorthosite residual magmas in the Laramie Anorthosite Complex, Wyoming. J Petrol 37:637–660
Morris PA (1984) Magfrac: a basic program for least-squares approximation of fractional crystallization. Comput Geosci 10:437–444
Morse SA (1982) A partisan review of Proterozoic anorthosites. Am Mineral 67:1087–1100
Owens BE, Dymek RF (1992) Fe-Ti-P-rich rocks and massif anorthosite; problems of interpretation illustrated from the Labrieville and St-Urbain plutons, Quebec. Can Mineral 30:163–190
Owens BE, Rockow MW, Dymek RF (1993) Jotunites from the Grenville Province, Quebec: petrological characteristics and implications for massif anorthosite petrogenesis. Lithos 30:57–80
Philpotts AR (1981) A model for the generation of massif-type anorthosites. Can Mineral 19:233–235
Powell JA, Gromet LP, Dymek RF (1982) Quartz monzodioritc and oxide–apatite-rich norites marginal to the StUrbain anorthosite massif: products of liquid immiscibility? Trans Am Geophys Union 63:456
Putirka KD (2005) Igneous thermometers and barometers based on plagioclase + liquid equilibria:tests of some existing models and new calibrations. Am Mineral 90:336–346
Putirka KD (2008) Thermometers and barometers for volcanic systems. Rev Mineral Geochem 69:61–120
Rämö OT (1991) Petrogenesis of Proterozoic rapakivi granites and related basic rocks of southeastern Fennoscandia: Nd and Pb isotopic and general geochemical constraints. Geol Surv Finl Bull 355:161
Rämö OT, Haapala I (1996) Rapakivi granite magmatism: a global review with emphasis on petrogenesis. In: Demaiffe D (ed) Petrology and geochemistry of magmatic suites of rocks in the continental and oceanic crusts. A volume dedicated to Professor Jean Michot. Université Libre de Bruxelles, Royal Museum for Central Africa
Rämö OT, Haapala I (2005) Rapakivi granites. In: Lehtinen M, Nurmi PA, Rämö OT (eds) Precambrian geology of Finland-key to the evolution of the fennoscandian Shield. Elsevier, Amsterdam, pp 533–562
Rämö OT, Turkki V, Mänttäri I, Heinonen A, Larjamo K, Lahaye Y (2014) Age and isotopic fingerprints of some plutonic rocks in the Wiborg rapakivi granite batholith with special reference to the dark wiborgite of the Ristisaari Island. Bull Geol Soc Finl 86:71–91
Roeder PL, Emslie RF (1970) Olivine-liquid equilibrium. Contrib Mineral Petrol 29:275–289
Sano Y, Terada K, Fukuoka T (2002) High mass resolution ion microprobe analysis of rare earth elemnts in silicate glass, apatite and zricon: lack of matrix dependency. Chem Geol 184:217–230
Savolahti A (1956) The Ahvenisto massif in Finland, the age of the surrounding gabbro-anorthosite complex and the crystallization of the rapakivi. Bulletin de la Comissione Geologique de Finlande 174
Savolahti A (1966) The differentiation of gabbro-anorthosite intrusions and the formation of anorthosites. C R Soc Géol Finl 38:173–197
Seifert KE, Dymek RF, Whitney PR, Haskin LA (2010) Geochemistry of massif anorthosite and associated rocks, Adirondacks Mountains, New York. Geosphere 6:855–899
Sun SS, McDonough WF (1989) Chemical and isotopic systematics of oceanic basalts: inplications for mantle composition and processes. Geol Soc 42:313–345
Taggart JE, Siems F (2002) Major elemental analysis by wavelength dispersive x-ray fluorescence spectrometry. U.S. Geological Survey Open File Report 02-223-T, pp 1–9
Vander Auwera J, Longhi J, Duchesne JC (1998) A liquid line of decent of the jotunite (hypersthene monzodiorite) suite. J Petrol 39:439–468
Watson BE (1979) Apatite saturation in basic to intermediate magmas. Geophys Res Lett 6:937–940
Whitney DL, Evans BW (2010) Abbreviations for names of rock-forming minerals. Am Mineral 95:185–187